

# IQA-Adapter: Exploring Knowledge Transfer from Image Quality Assessment to Diffusion-based Generative Models

Abud Khaled<sup>1,3</sup>, Sergey Lavrushkin<sup>1,2</sup>, Alexey Kirillov<sup>3,4</sup>, Dmitriy Vatolin<sup>1,2,3</sup>

<sup>1</sup>MSU Institute for Artificial Intelligence

<sup>2</sup>ISP RAS Research Center for Trusted Artificial Intelligence

<sup>3</sup>Lomonosov Moscow State University

<sup>4</sup>Yandex

{khaled.abud, sergey.lavrushkin, alexey.kirillov, dmitriy}@graphics.cs.msu.ru

## Abstract

*Diffusion-based models have recently transformed conditional image generation, achieving unprecedented fidelity in generating photorealistic and semantically accurate images. However, consistently generating high-quality images remains challenging, partly due to the lack of mechanisms for conditioning outputs on perceptual quality. In this work, we propose methods to integrate image quality assessment (IQA) models into diffusion-based generators, enabling quality-aware image generation.*

*First, we experiment with gradient-based guidance to optimize image quality directly and show this approach has limited generalizability. To address this, we introduce **IQA-Adapter**, a novel architecture that conditions generation on target quality levels by learning the relationship between images and quality scores. When conditioned on high target quality, IQA-Adapter shifts the distribution of generated images towards a higher-quality subdomain. This approach achieves up to a 10% improvement across multiple objective metrics, as confirmed by a subjective study, while preserving generative diversity and content. Additionally, IQA-Adapter can be used inversely as a degradation model, generating progressively more distorted images when conditioned on lower quality scores. Our quality-aware methods also provide insights into the adversarial robustness of IQA models, underscoring the potential of quality conditioning in generative modeling and the importance of robust IQA methods.*

## 1. Introduction

Recent advances in diffusion-based image generation have led to a new wave of powerful text-to-image models, capable of producing realistic and highly detailed images from text prompts. Models such as DALL-E 3 [6], FLUX [43],

and SDXL [58] exemplify this success, establishing new standards in visual fidelity and alignment with user intent. Beyond text prompts, recent studies have extended the conditioning flexibility of generative models by incorporating additional guidance sources such as depth [91], pose [91], and images [87], expanding the expressive capacity of these models and enabling greater control over generation outputs. This development has also sparked interest in unified approaches, with recent work like OmniGen [83] proposing universal models that integrate diverse conditioning types natively.

Despite these advances, one area that remains largely unexplored in the context of conditional generative modeling is image quality and aesthetics assessment (IQA/IAA). IQA, a specialized field within computer vision, focuses on evaluating image quality in ways that align closely with human perception. While closely related, IAA emphasizes aesthetic attributes that are often dependent on the content of the image. In this work, we aim to bridge the gap between generative modeling and IQA/IAA by incorporating IQA-driven conditioning, enabling improvements in generated image quality while preserving content fidelity.

Aligning generative models with human preferences in terms of image quality has strong practical motivation. While current evaluations of generative models primarily focus on image-text alignment or distributional closeness to real data, image quality has received relatively little attention. Although some recent approaches [41, 82, 85] have started to address the alignment of generated content with both textual and aesthetic human preferences, very few attempts, if any, have directly incorporated existing IQA/IAA expertise into generative models. This lack of integration persists despite expanding research [15, 21, 45, 81] that leverages generative priors from diffusion-based models to advance IQA methods, indicating promising potential for knowledge transfer between the fields.

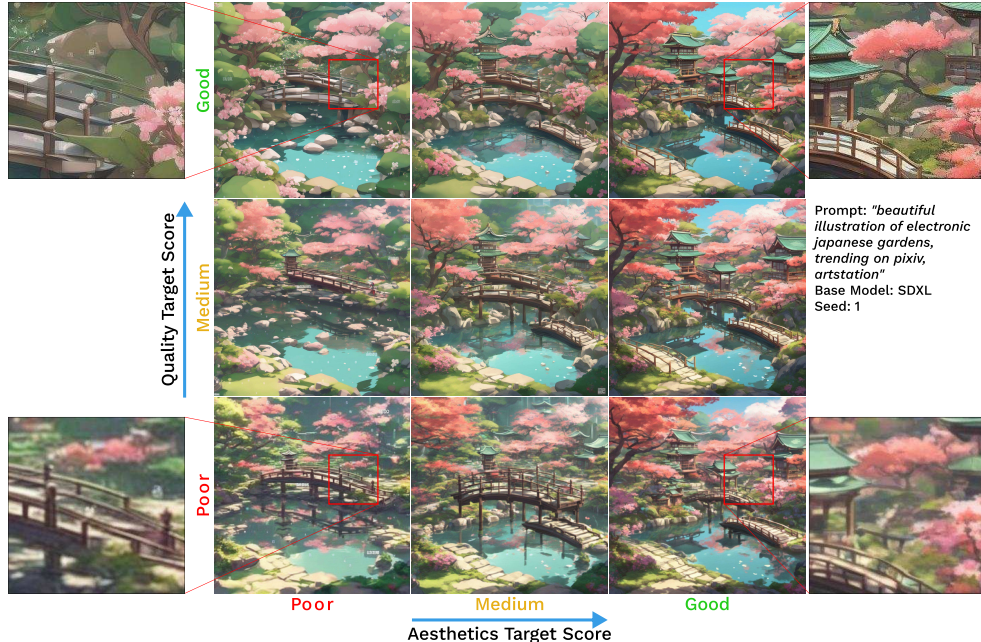


Figure 1. Quality-aware image generation with **IQA-Adapter**. All images are generated with the SDXL base model, the same prompt, and the seed. The IQA-Adapter is trained with TOPIQ [10] and LAION-Aesthetics [67] metrics.

We summarize our contributions as follows:

- **Advancement in IQA-driven generation.** To our knowledge, this work is the first systematic attempt to employ IQA knowledge in a diffusion-based generation, establishing a foundation for further research at the intersection of IQA and generative modeling.
- **IQA-Adapter architecture.** We introduce IQA-Adapter, a novel adapter-based conditioning architecture for diffusion models that enables quality-aware generation guided by IQA/IAA scores.
- **Diverse IQA/IAA model integration.** We experiment with a range of IQA and IAA models with diverse architectures and training datasets, demonstrating the adaptability of our approach to different quality and aesthetic metrics and the generalization of quality features learned by IQA-Adapter. Furthermore, we employ a gradient-based quality optimization method to explore adversarial patterns that emerge within images generated with a high IQA-guidance scale. Our findings also shed light on the interactions between IQA models and generated images, identifying features that enhance perceived quality and uncovering potential biases in IQA models.

## 2. Related work

**Generative Models.** Various approaches have been explored in the field of image generation, including generative adversarial networks (GANs) and variational autoencoders (VAEs), which dominated early progress in the

area. Recently, however, diffusion models have emerged as the state-of-the-art approach for image generation. Pioneering works such as [61, 62, 64] established diffusion models as superior to previous methods, introducing the first production-grade models capable of generating high-quality images. Following these advancements, further research focused on improving aspects such as image relevance, aesthetic appeal, and overall quality. Studies [5, 6, 12, 14, 19, 38, 43, 49] contributed to these improvements through enhancements in data quality, model scaling, architectural refinement, and the exploration of alternative diffusion frameworks.

**Adapters and customization.** Advances in diffusion models have led to the development of new techniques that enhance control over the image generation process. LoRA [34] introduced a parameter-efficient fine-tuning method that updates only a low-rank decomposition of model weights, enabling easy model customization and stylization. Methods like Dreambooth [63] and Textual Inversion [22] further enabled personalization by allowing diffusion models to generate outputs tailored to specific user inputs. IP-Adapter [87] extended these works for universal image variation. Additionally, ControlNet [91] and T2IAdapter [55] incorporated spatial conditioning into diffusion models by using supplementary networks to encode specific conditions. Furthermore, ConceptSliders [23] introduced an approach for training adapters that can adjust particular attributes within generated images. Most of these techniques, however, focus on conditioning image generation through

text, images, or binary masks. In contrast, our work proposes a novel adapter that enables conditioning based on numerical inputs, which represent continuous image attributes such as aesthetics or quality.

Several methods explored conditioning on technical attributes to guide content generation, leveraging specific parameters to influence the output [3, 58, 59]. For example, SDXL [58] incorporated image size and crop parameters to enhance pretraining. However, these approaches focus primarily on low-level technical attributes. In contrast, our approach introduces conditioning on high-level semantic attributes, which are automatically extracted using pre-trained, task-specific models.

**IQA and IAA.** Image quality assessment (IQA) focuses on evaluating the technical quality of images by analyzing distortions, artifacts, and other degradations that affect visual perception. IQA methods are typically classified into full-reference (FR) and no-reference (NR) approaches, depending on whether a pristine reference image is available. In contrast, image aesthetics assessment (IAA) deals with subjective judgments about an image’s visual appeal, considering factors such as composition, lighting, color harmony, and overall artistic impression.

Early IQA/IAA methods relied on explicitly modeling human perception, scene statistics, or using handcrafted similarity metrics [52–54, 70, 79, 80, 90]. These approaches were limited by the complexities and incomplete understanding of the human visual system. Modern techniques [2, 11, 28, 36, 40, 57, 75, 76, 78, 86, 94] have shifted toward machine learning, particularly deep learning models, which are trained on large datasets with human-provided opinion scores [20, 24, 33, 35, 42, 47, 56, 88]. Recent advancements also include diffusion-based approaches [15, 21, 45, 81], which used generative model priors to enhance the robustness and accuracy of quality assessments. Unlike these approaches, which transfer knowledge from generative models to improve IQA, our work reverses this direction by integrating IQA knowledge into diffusion-based generative models, thereby enriching the generative process with quality-focused insights

### 3. Learning the relationship between images and visual quality from IQA models

#### 3.1. Baselines

To establish a simple baseline for integrating IQA model knowledge into the generation process, we introduce a technique inspired by classifier guidance [17]. In our adaptation, we leverage NR-IQA models rather than a classifier, interpreting IQA scores as soft probabilities that reflect the likelihood of an image achieving high perceptual quality. This approach uses feedback from the IQA model to iteratively

optimize image quality during the generation process:

$$\hat{\epsilon}_\theta(z_{t-1}|c_t, f_\phi) = \epsilon_\theta(z_t|c_t) + \alpha \cdot \omega(t) \nabla_{z_t} \log f_\phi(D(z_t)),$$

where  $\epsilon_\theta$  is a latent diffusion model,  $c_t$  is a textual condition,  $f_\phi$  is a NR metric,  $z_t$  represents the latent image at the  $t$ -th diffusion step, and  $D(\cdot)$  is the VAE’s decoder that maps the latent representation back to image space. The parameter  $\alpha$  allows adjustment of the IQA guidance weight, balancing the impact of quality conditioning, while the scaling coefficient  $\omega(t)$  modulates the gradient’s influence over time, linearly increasing from 0 to 1.

Although this method optimizes the target IQA score, its reliance on gradient-based adjustments introduces the risk of exploiting vulnerabilities within the IQA model. This can result in images that receive high ratings from the IQA model yet exhibit noticeable visual distortions — a phenomenon similar to adversarial attacks, which we further discuss in Section 5.2.

Another naive approach involves fine-tuning the generative model on data of the target quality. This method, however, lacks flexibility for controlling the generative process during inference and can affect the generative capabilities of the original model.

#### 3.2. IQA-Adapter

To address limitations of inference-time gradient optimization, we propose a method that implicitly learns a relationship between images and their corresponding quality assessments. By learning this connection, the generative model can internalize features associated with target-quality images and avoid characteristics linked to opposite quality. For instance, when conditioned on high-quality parameters, the model should generate images with fine-grained details and vibrant colors. Conversely, when conditioned on low quality, it should produce artifacts such as JPEG compression distortions or blurring.

##### 3.2.1. Architecture

To condition the generative model on image quality, we leverage IP-Adapter [87] technique, which supports image-prompt conditioning in pretrained text-to-image diffusion models. The IP-Adapter operates by projecting the CLIP embedding of an image prompt into additional tokens, which are then integrated into the model via cross-attention mechanisms. This method enables the base model to receive detailed conditioning information from non-textual sources without altering its core weights. We selected this architecture for its lightweight design, ability to preserve core model’s weights, and minimal computational overhead during training and inference.

As illustrated in Figure 2, we repurpose the IP-Adapter framework to pass visual quality scores as conditioning information into the generative model. We refer to this modified approach as **IQA-Adapter**. In this setup, quality scores

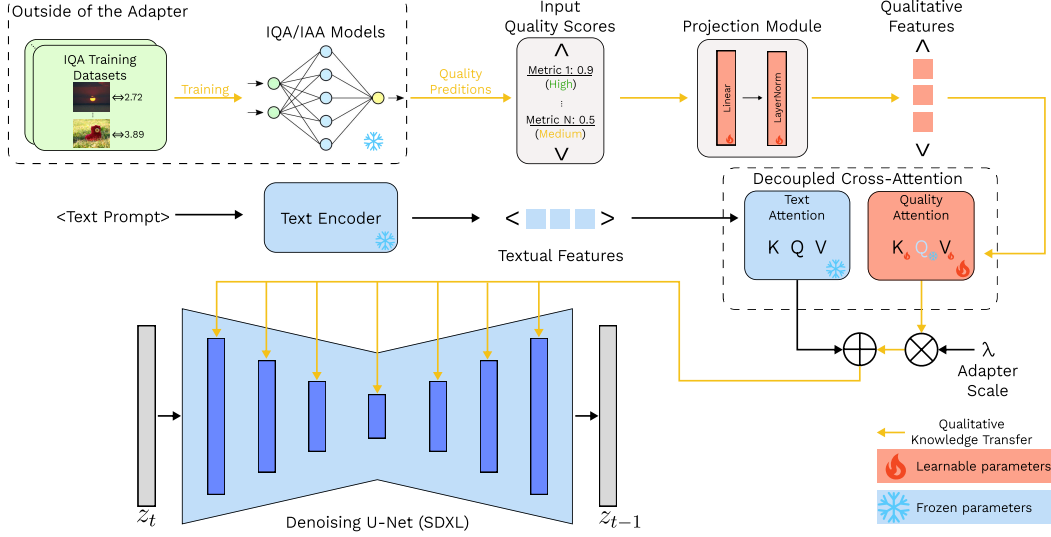


Figure 2. Overall architecture of the proposed **IQA-Adapter**. Yellow arrows demonstrate the flow of knowledge from IQA/IAA models to diffusion-based generator.

are projected into tokens matching the dimensionality of textual tokens through a small projection module, consisting of a linear layer and LayerNorm [4]. These tokens then enter the main generative model (U-Net in SDXL [58]) via cross-attention layers, allowing the model to adjust image quality based on specified IQA scores.

IQA-Adapter can accept multiple IQA scores as input, allowing for the integration of various IQA/IAA models that capture different aspects of image fidelity, e.g., quality in terms of distortions and overall aesthetics of the image. To ensure consistency, all metric values are standardized to have zero mean and unit variance based on the training dataset.

A key feature of IQA-Adapter, inherited from the IP-Adapter, is its **Decoupled Cross-Attention** mechanism, which enables the model to process adapter tokens separately from textual prompt tokens. Specifically, the adapter adds an additional cross-attention layer for each existing cross-attention operation in the base model. Without an adapter, the base model processes the textual conditioning  $c_t$  as follows:

$$\text{Attention}(Z, c_t) = \text{Softmax}\left(\frac{QK^T}{\sqrt{d}}\right)V$$

where  $Q = ZW_q$ ,  $K = c_tW_k$ ,  $V = c_tW_v$ ,  $Z$  are image features and  $d$  is the projection space dimension. When the adapter is added, the attention mechanism is modified as follows:

$$\text{DecAttention}(Z, c_t, c_q) = \text{Softmax}\left(\frac{QK^T}{\sqrt{d}}\right)V + \lambda \times \text{Softmax}\left(\frac{QK'^T}{\sqrt{d}}\right)V'$$

where  $K' = c_qW'_k$ ,  $V' = c_qW'_v$ , and  $c_q$  are the quality conditioning features. Notably, the query matrix  $W_q$  that processes the generated image features  $Z$  is shared across both attention operations. This setup allows the IQA-Adapter to learn and apply quality-specific attributes independently from the text-based conditioning and generalize them across various textual contexts. To control the strength of the IQA-Adapter during inference, we introduce a scaling parameter  $\lambda$ , which adjusts the impact of quality conditioning by modifying the cross-attention term for quality features.

### 3.2.2. IQA-Adapter Training

We train IQA-Adapter on triplets (image, text, input quality scores) where the image-text pairs are drawn from a text-to-image dataset, and the quality scores are estimated by passing each image through a target IQA/IAA model. The training follows the standard denoising diffusion probabilistic model (DDPM) procedure [32]. In this process, a random timestep  $t \sim U[0, 1]$  is sampled, and noise is incrementally applied to the image  $x$  at the corresponding noise scale. The model then learns to predict the added noise with the following objective:

$$\mathcal{L} = \mathbb{E}_{x,t,\epsilon} [\|\epsilon - \epsilon_\theta(x_t|c_t, c_q)\|^2]$$

where  $x_t$  is a noised representation of the input image,  $c_t$  is the textual condition,  $c_q$  is the qualitative condition,  $\epsilon$  is the added noise, and  $\epsilon_\theta(x_t|c_t, c_q)$  is the predicted noise.

During this process, only the adapter weights are adjusted to allow the generative model to incorporate quality score information and steer the output generation accordingly. To maintain flexibility for classifier-free guidance during inference, we randomly drop the textual and qual-



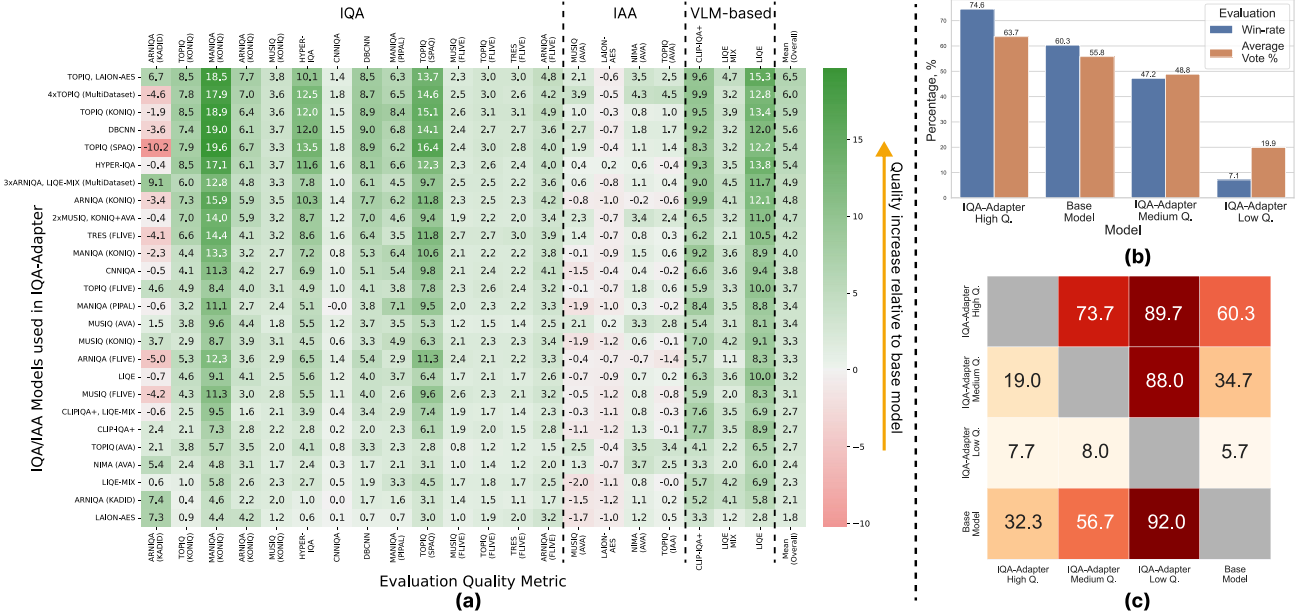


Figure 3. (a) Quality improvement relative to generation without the adapter (in %) for the IQA-Adapters trained on different IQA/IAA models. All IQA-Adapters are conditioned with high target quality (99th percentile of the training dataset) and use the same prompts and seeds. Prompts are taken from Lexica.art user-generated prompts dataset. (b,c) Results of the side-by-side subjective study of the IQA-Adapter conditioned on different quality levels. (b) Overall results of all comparisons. (c) Pair-wise win rates for each quality level.

ity conditions with a small probability, which encourages the model to generate images unconditionally.

A key advantage of IQA-Adapter is that it does not require backpropagation through the IQA models (as it only uses quality scores of training images), enabling the use of non-differentiable metrics or even ground-truth subjective scores from sufficiently large subjective studies. As demonstrated in Section 4.2, bypassing gradient-based optimization significantly improves the transferability across metrics beyond those used for training, enhancing the generality of the learned quality features across various evaluation models.

## 4. Experiments and Evaluation

### 4.1. Experimental Setup

**Models.** For all experiments involving both gradient-based guidance and IQA-Adapter, we used SDXL as the base model. The IQA-Adapters were trained on the CC3M [69] dataset ( $\sim 3$  million images) for 24,000 steps with a learning rate of  $1 \times 10^{-4}$ , followed by fine-tuning on a subset [16] of the LAION-5B [68] dataset ( $\sim 170k$  images with an aesthetics score  $> 6.5$ ) for an additional 3,000 steps with a reduced learning rate of  $1 \times 10^{-5}$ . We employed two tokens for qualitative features. For more details on the IQA-Adapter training, refer to the supplementary materials Section 9.

During inference, we used a guidance scale of 7.5 and 35 sampling steps. For the IQA-Adapters, we set the adapter

scale to  $\lambda = 0.5$ , while for the gradient-based method, we applied a quality-guidance scale of  $\alpha = 30$ .

Our experiments were conducted on a cluster equipped with Nvidia Ampere series GPUs. Training a single IQA-Adapter model required approximately 260 Nvidia A100 80GB GPU hours.

**IQA/IAA Models.** We experimented with a diverse set of 22 state-of-the-art quality assessment models, varying in architecture and training dataset. The models include CNN-based approaches like ARNIQA [1], NIMA [77], DBCNN [93], and CNNIQA [37]; TOPIQ [10], which combines a CNN backbone with an attention mechanism; HYPER-IQA [74], which leverages a hyper-network with a CNN. Additionally, we tested transformer-based models, including MUSIQ [39], TRES [27], and MANIQA [86] and metrics integrating vision-language capabilities like LIQE[95], LIQE-MIX[95] and CLIP-IQA+[78]. Where available, multiple versions of some models were tested, each trained on different datasets. Table 2 in the supplementary materials lists all employed metrics with their corresponding training datasets.

**Evaluation Datasets.** We use several diverse prompt datasets for model evaluation:

- *Qualitative evaluation:* A filtered subset of 8,200 user-generated prompts from Lexica.art website [66] and PartiPrompts [89] (1,600 prompts of different aspects and challenges).
- *Generative and compositional capabilities evaluation:*

GenEval benchmark [25] and corresponding prompts.

- *Additional fidelity measures:* A subset of 10,000 captions from MS COCO [48] for FID [31] and related scores.

The code for training and inference, as well as pre-trained weights for the IQA-Adapters, will be available in our GitHub repository: <https://github.com/X1716/IQA-Adapter>.

## 4.2. High-quality conditioning

To evaluate the effectiveness of knowledge transfer from IQA models to diffusion-based generative models, we first explore the high-quality conditioning scenario, as this is the primary application for quality-aware generation. To assess improvements objectively, we calculate the relative gain in quality scores compared to the base model:

$$\text{RelGain} = \frac{1}{N} \sum_{i=0}^N \frac{f(x'_i) - f(x_i)}{f(x_i)} \cdot 100\%$$

where  $f(x)$  represents the quality assessment model, and  $x_i$  and  $x'_i$  are images generated under the same prompt and seed for the base and quality-conditioned models, respectively.

Detailed results for PartiPrompts dataset and the gradient-based method are provided in the supplementary materials (see Sections 10.1, 10.2). The gradient-based method, which directly optimizes IQA scores, increases target scores but fails to improve other IQA/IAA metrics, likely due to adversarial exploitation of model-specific vulnerabilities. Given its limitations, we focus on IQA-Adapter in the remaining experiments, discussing the gradient-based method as a potential white-box adversarial attack in Section 5.2.

For IQA-Adapter, high-quality conditioning is achieved by setting the input to the 99-th percentile of the target metric’s values from the training dataset. Separate IQA-Adapters were trained for each IQA/IAA metric, and a multi-metric approach was tested by conditioning on combinations of different IQA/IAA models. Figure 3(a) shows the relative gains for various IQA-Adapters on user-generated prompts from the Lexica.art dataset.

Unlike the gradient-based approach, the IQA-Adapters trained even on single IQA models show consistent quality gains across multiple metrics, with an average improvement of 4-6% over the base model. Notably, gains for the target metric do not significantly exceed those for other metrics, demonstrating strong cross-metric transferability.

IQA scores tend to improve more easily than IAA scores, likely because IQA focuses on perceptual quality attributes that are less dependent on composition, whereas IAA is more content-sensitive and requires adjustments in both text and quality conditions.

Using multiple IQA/IAA metrics enhances the IQA-Adapter’s performance across evaluation metrics. For ex-

ample, combinations like TOPIQ and LAION-AES models, and multiple versions of TOPIQ (see “4×TOPIQ” row on Figure 3(a)), exhibit the best transferability, suggesting that diverse metrics provide richer quality information, broadening the IQA-Adapter’s capacity to capture complex quality attributes. Quality improvements are further supported by a subjective study detailed in Section 4.3.1.

## 4.3. Alignment with qualitative condition

To assess the alignment between input quality conditions provided to the IQA-Adapter during generation and the quality of generated images, we attempt to condition it on different percentiles of the target IQA model’s values on the training dataset. Figure 4 demonstrates the impact of quality-condition on IQA scores and examples of images generated for corresponding quality levels. The results indicate a gradual increase in quality scores from the IQA model as the input condition rises, with generated images appearing progressively sharper and more detailed. We exemplify more quality conditions for the IQA-Adapters trained with different IQA/IAA models in supplementary Section 18.

### 4.3.1. Subjective Study

To confirm that image quality improves with input quality conditions, we conducted a subjective study with the IQA-Adapter conditioned on three quality levels: low (1st percentile), medium (50th percentile), and high (99th percentile), as well as the base model (SDXL-Base). We utilized the IQA-Adapter conditioned on TOPIQ and LAION-AES models, which showed the highest average IQA/IAA metric increases (Figure 3(a)). Participants evaluated the visual quality of images generated from 300 prompts, contributing over 22,300 responses from 1,017 users, with each image pair evaluated by at least 10 unique users (12.1 on average). For each model, we calculated the overall win rate defined as a share of image pairs on which it achieved the majority of votes. Additionally, we demonstrate the average percent of votes for the model across all image-pairs. Results are shown in Figure 3(b), and pairwise win rates in Figure 3(c). For more details on the subjective study, see supplementary Section 15.

Win rates align well with input quality conditions: high-quality conditions achieve the highest win rate, followed by medium- and low-quality. As shown in Figure 3(c), the IQA-Adapter conditioned on high quality outperforms the base model with 60% win rate, compared to 32% for the base model (~7% were rated equally). This demonstrates that IQA-Adapter effectively captures and reproduces qualitative concepts aligned with human image quality judgments. Notably, the win rate for the low-quality condition drops significantly compared to medium quality. Figure 4(a) further indicates that objective quality decreases sharply below the 25th percentile.

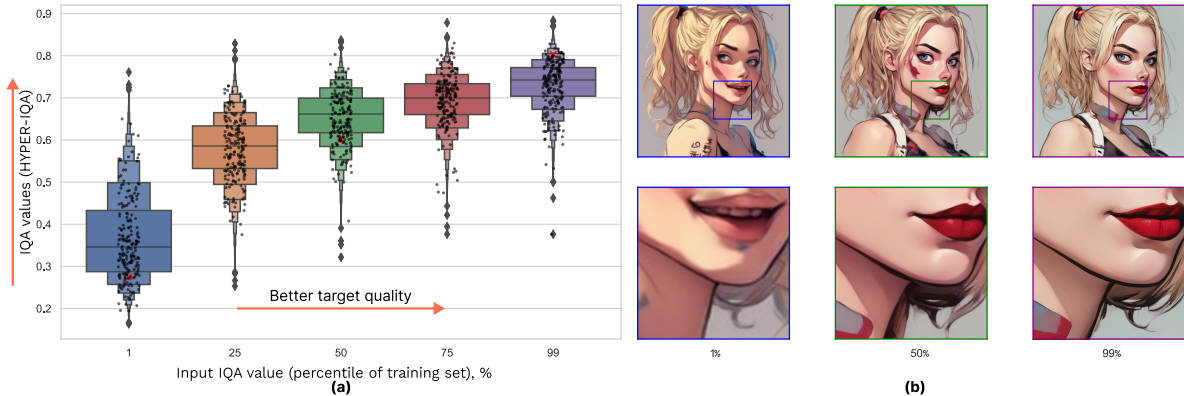


Figure 4. (a) Distributions of quality scores for images generated with the IQA-Adapter conditioned on different target quality levels (1-99 percentiles of the training dataset). The adapter is trained with the HYPER-IQA metric. (b) Examples of images generated with different target quality.

Models in IQA-Adapter	Two Object <sup>†</sup>	Attribute Binding <sup>†</sup>	Colors <sup>†</sup>	Counting <sup>†</sup>	Single Object <sup>†</sup>	Position <sup>†</sup>	Overall <sup>†</sup>
MANIQA (PIPAL)	73.23%	20.25%	86.17%	36.56%	96.56%	10.50%	53.88%
TOPIQ (KONIQ)	71.97%	18.75%	85.11%	38.75%	98.12%	13.75%	54.41%
CLIP-IQA+, LIQE-MIX	71.72%	20.25%	85.64%	41.25%	97.81%	11.75%	54.74%
TOPIQ, LAION-AES	69.70%	18.75%	85.90%	45.31%	99.38%	13.00%	55.34%
3xARNIQA, LIQE-MIX (MultiDataset)	<b>73.99%</b>	19.25%	<b>89.36%</b>	39.69%	<b>99.69%</b>	13.75%	55.95%
CLIP-IQA+	72.73%	22.75%	88.03%	43.44%	98.44%	12.25%	56.27%
HYPER-IQA	73.99%	<b>25.25%</b>	85.90%	39.69%	98.75%	<b>14.75%</b>	<b>56.39%</b>
TOPIQ (FLIVE)	72.73%	21.75%	87.77%	<b>45.94%</b>	99.38%	13.00%	<b>56.76%</b>
Base Model	73.74%	21.75%	<b>88.30%</b>	43.75%	<b>99.69%</b>	10.50%	56.29%

Table 1. Results of the IQA-Adapters trained with different IQA/IAA models on GenEval benchmark. Percents represent the accuracy of object-detection model on generated images. Results for all evaluated adapters are available in supplementary Table 4.

#### 4.4. Evaluating generative capabilities

To evaluate the generative capabilities of the quality-conditioned model and ensure that it doesn’t affect the ability to follow the textual prompt and generate diverse images, we tested it on the GenEval benchmark. It uses an object-detection model to evaluate the alignment between generated images and textual conditions. Table 1 shows the comparison results. Overall scores for most adapters are close to those of the base model. For each evaluation criterion, there is an IQA-Adapter that consistently outperforms the base model. The IQA-Adapter trained with HYPER-IQA, for example, increases “Attribute binding” (rendering two objects with two different colors) and “Position” (rendering two objects with specific relative positions) scores, suggesting better alignment with complex compositional prompts. The least improvement is in “Counting,” likely due to some IQA-Adapters’ tendency to add small details that sometimes increase object counts unnecessarily.

Additionally, we calculated FID, IS [65] and CLIP [30] scores for all tested adapters on a 10,000 captions subset of MS COCO. The results can be found in supplementary Sec-

tion 11. In summary, these findings indicate that the adapter conditioned on high quality mostly retains the generative capabilities of the base model, while shifting the generation towards a higher-quality subdomain.

## 5. Discussion and Future Work

### 5.1. IQA-Adapter as a degradation model

As most IQA models are trained to assess distorted images, they can reliably detect noise, compression, blur, and other artifacts on images during IQA-Adapter training. Therefore, this knowledge is transferred to the generative model and such image attributes are connected with low-quality conditions. This allows IQA-Adapter to generate progressively more distorted images as input quality-condition decreases. The IQA-Adapter in Figure 4(b), for example, implicitly learned to simulate JPEG compression artifacts when conditioned on low quality (1st percentile of the training dataset). As IQA models are mostly tailored to assess low-level quality attributes (in contrast with IAA methods), images produced with different quality levels usually retain similar content and composition, as illustrated in Figure 1 (bottom-to-top direction).

By applying appropriate filtering to exclude image pairs with unintended content differences, IQA-Adapter can generate large synthetic datasets of distorted and corresponding high-quality images. Such datasets can subsequently be used to pretrain models for image enhancement, deblurring, and other restoration tasks. While training such methods is a subject for future work, we additionally explore the distances between generated images with different target-quality conditions in supplementary Section 13.2. We also note that IQA-Adapter can be additionally fine-tuned with unpaired data containing specific distortions to simulate them during inference.



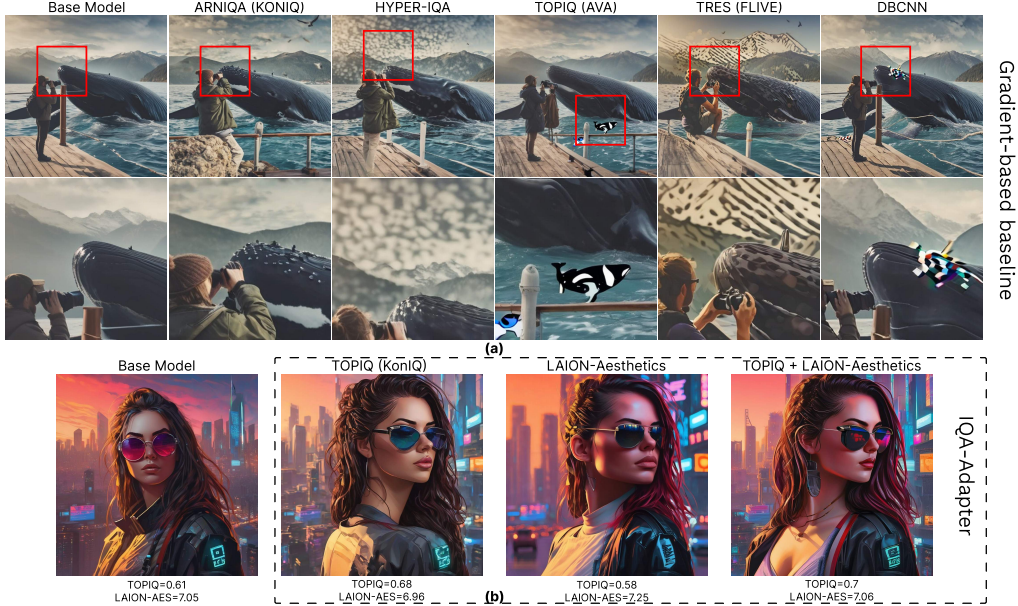


Figure 5. (a) Examples of adversarial patterns appearing under high **gradient-based** guidance scale. (b) Examples of images generated with the **IQA-Adapters** trained with different IQA models. Each IQA/IAA model has its stylistic preferences. All images in each line are generated with the same prompt and seed.

## 5.2. Exploring adversarial patterns, biases, and preferences of IQA models

When applied with a sufficiently high guidance scale, the gradient-based method can exploit vulnerabilities of the target IQA model, artificially inflating its values and shifting the generation towards an adversarial subdomain. This approach tends to produce images with distinct patterns specific to each IQA model. Figure 5(a) demonstrates adversarial patterns generated with different guidance models. For certain models, such as TRES and HYPER-IQA, these patterns form grid-like structures, and for others, like TOPIQ and DBCNN, they concentrate in smaller regions. We present more adversarial examples generated with gradient-based guidance and GradCAM [26] visualizations of corresponding IQA models in supplementary.

Our study further reveals that most IQA models exhibit distinct preferences when used with a high IQA-Adapter scale. For instance, TOPIQ often favors sharper images, while LAION-AES tends to enhance color saturation, producing more vibrant visuals. These effects can be compounded by using multiple IQA/IAA models simultaneously during adapter training, as illustrated in Figure 5(b).

Furthermore, in supplementary Section 8 we explore the use of negative-quality guidance, similar to negative text-prompt guidance. It magnifies the impact of the adapter by subtracting the noise prediction associated with the opposite quality condition during generation. When provided with a strong negative-quality condition, the adapter attempts to remove certain fine-grained details, often pro-

ducing "overly-stylized" image with sharp outlines around the edges (see supplementary Figure 7). Such images tend to achieve very high quality scores across multiple metrics, but this rarely corresponds to a real quality increase. This observation suggests that, under such conditions, IQA-Adapter exploits the preferences of IQA models to artificially boost quality scores. This underscores the potential of IQA-Adapter as a black-box tool for investigating the adversarial robustness and biases of IQA models in future research.

We further discuss the limitations of IQA-Adapter in supplementary Section 14.

## 6. Conclusion

In this work, we explored different techniques to transfer knowledge from image quality assessment models to diffusion-based image generators. We proposed a novel IQA-Adapter architecture that allows the generator model to learn implicit connections between images and corresponding quality levels and enables quality-aware generation. Experiments and subjective evaluation showed that IQA-Adapter efficiently conditions the generation process in a way that aligns with human judgment, all while retaining the generative capabilities of the base model. Additionally, we demonstrate various use cases of IQA-conditioned generation, including the exploration of adversarial robustness, preferences, and biases of IQA/IAA models and image degradation.



## References

- [1] Lorenzo Agnolucci, Leonardo Galteri, Marco Bertini, and Alberto Del Bimbo. Arnika: Learning distortion manifold for image quality assessment. In *Proceedings of the IEEE/CVF Winter Conference on Applications of Computer Vision*, pages 189–198, 2024. 5
- [2] Lorenzo Agnolucci, Leonardo Galteri, Marco Bertini, and Alberto Del Bimbo. Arnika: Learning distortion manifold for image quality assessment. In *Proceedings of the IEEE/CVF Winter Conference on Applications of Computer Vision*, pages 189–198, 2024. 3
- [3] Eloi Alonso, Adam Jelley, Vincent Micheli, Anssi Kanervisto, Amos Storkey, Tim Pearce, and François Fleuret. Diffusion for world modeling: Visual details matter in atari. *arXiv preprint arXiv:2405.12399*, 2024. 3
- [4] Jimmy Lei Ba, Jamie Ryan Kiros, and Geoffrey E. Hinton. Layer normalization. <https://arxiv.org/abs/1607.06450>, 2016. 4
- [5] Jason Baldridge, Jakob Bauer, Mukul Bhutani, Nicole Brich-tova, Andrew Bunner, Kelvin Chan, Yichang Chen, Sander Dieleman, Yuqing Du, Zach Eaton-Rosen, et al. Imagen 3. *arXiv preprint arXiv:2408.07009*, 2024. 2
- [6] James Betker, Gabriel Goh, Li Jing, Tim Brooks, Jianfeng Wang, Linjie Li, Long Ouyang, Juntang Zhuang, Joyce Lee, Yufei Guo, et al. Improving image generation with better captions. <https://cdn.openai.com/papers/dall-e-3.pdf>, 2023. 1, 2
- [7] Eyal Betzalel, Coby Penso, Aviv Navon, and Ethan Fetaya. A study on the evaluation of generative models. *arXiv preprint arXiv:2206.10935*, 2022. 5
- [8] Artem Borisov, Evgeney Bogatyrev, Egor Kashkarov, and Dmitriy Vatolin. Msu video super-resolution quality metrics benchmark 2023. URL: <https://videoprocessing.ai/benchmarks/super-resolution-metrics.html>, 2023. Date of access: 2024-11-19. 6
- [9] Chaofeng Chen and Jiadi Mo. IQA-PyTorch: Pytorch toolbox for image quality assessment. [Online]. Available: <https://github.com/chaofengc/IQA-PyTorch>, 2022. 1
- [10] Chaofeng Chen, Jiadi Mo, Jingwen Hou, Haoning Wu, Liang Liao, Wenxiu Sun, Qiong Yan, and Weisi Lin. Topiq: A top-down approach from semantics to distortions for image quality assessment. *IEEE Transactions on Image Processing*, 2024. 2, 5
- [11] Chaofeng Chen, Jiadi Mo, Jingwen Hou, Haoning Wu, Liang Liao, Wenxiu Sun, Qiong Yan, and Weisi Lin. Topiq: A top-down approach from semantics to distortions for image quality assessment. *IEEE Transactions on Image Processing*, 2024. 3
- [12] Junsong Chen, Chongjian Ge, Enze Xie, Yue Wu, Lewei Yao, Xiaozhe Ren, Zhongdao Wang, Ping Luo, Huchuan Lu, and Zhenguo Li. Pixart- $\sigma$ : Weak-to-strong training of diffusion transformer for 4k text-to-image generation. *arXiv preprint arXiv:2403.04692*, 2024. 2
- [13] Alexandre Ciancio, Eduardo AB da Silva, Amir Said, Ramin Samadani, Pere Obrador, et al. No-reference blur assessment of digital pictures based on multifeature classifiers. *IEEE Transactions on image processing*, 20(1):64–75, 2010. 2
- [14] Xiaoliang Dai, Ji Hou, Chih-Yao Ma, Sam Tsai, Jialiang Wang, Rui Wang, Peizhao Zhang, Simon Vandenhende, Xiao-fang Wang, Abhimanyu Dubey, et al. Emu: Enhancing image generation models using photogenic needles in a haystack. *arXiv preprint arXiv:2309.15807*, 2023. 2
- [15] Diptanu De, Shankhanil Mitra, and Rajiv Soundararajan. Genzika: Generalized image quality assessment using prompt-guided latent diffusion models. *arXiv preprint arXiv:2406.04654*, 2024. 1, 3
- [16] Bhargav Desai. Laion-5b 170k subset of images with aesthetics score > 6.5. [https://huggingface.co/datasets/bhargavsdesai/laion\\_improved\\_aesthetics\\_6.5plus\\_with\\_images](https://huggingface.co/datasets/bhargavsdesai/laion_improved_aesthetics_6.5plus_with_images), 2022. 5
- [17] Prafulla Dhariwal and Alex Nichol. Diffusion models beat gans on image synthesis. In *Proceedings of the 35th International Conference on Neural Information Processing Systems*, Red Hook, NY, USA, 2024. Curran Associates Inc. 3
- [18] Keyan Ding, Kede Ma, Shiqi Wang, and Eero P. Simoncelli. Image quality assessment: Unifying structure and texture similarity. *CoRR*, abs/2004.07728, 2020. 6
- [19] Patrick Esser, Sumith Kulal, Andreas Blattmann, Rahim Entezari, Jonas Müller, Harry Saini, Yam Levi, Dominik Lorenz, Axel Sauer, Frederic Boesel, et al. Scaling rectified flow transformers for high-resolution image synthesis, march 2024. URL <http://arxiv.org/abs/2403.03206>. 2
- [20] Yuming Fang, Hanwei Zhu, Yan Zeng, Kede Ma, and Zhou Wang. Perceptual quality assessment of smartphone photography. In *Proceedings of the IEEE/CVF conference on computer vision and pattern recognition*, pages 3677–3686, 2020. 3, 2
- [21] Honghao Fu, Yufei Wang, Wenhan Yang, and Bihan Wen. Dp-iqa: Utilizing diffusion prior for blind image quality assessment in the wild. *arXiv preprint arXiv:2405.19996*, 2024. 1, 3
- [22] Rinon Gal, Yuval Alaluf, Yuval Atzmon, Or Patashnik, Amit Haim Bermano, Gal Chechik, and Daniel Cohen-or. An image is worth one word: Personalizing text-to-image generation using textual inversion. In *ICLR*, 2023. 2
- [23] Rohit Gandikota, Joanna Materzyńska, Tingrui Zhou, Antonio Torralba, and David Bau. Erasing concepts from diffusion models. In *ECCV*, 2024. *arXiv preprint arXiv:2311.12092*. 2
- [24] Deepti Ghadiyaram and Alan C Bovik. Massive online crowdsourced study of subjective and objective picture quality. *IEEE Transactions on Image Processing*, 25(1):372–387, 2015. 3, 2
- [25] Dhruba Ghosh, Hannaneh Hajishirzi, and Ludwig Schmidt. Geneval: An object-focused framework for evaluating text-to-image alignment. *NeurIPS*, 36, 2024. 6
- [26] Jacob Gildenblat and contributors. Pytorch library for cam methods. <https://github.com/jacobgil/pytorch-grad-cam>, 2021. 8
- [27] S Alireza Golestaneh, Saba Dadsetan, and Kris M Kitani. No-reference image quality assessment via transformers, relative ranking, and self-consistency. In *Proceedings of the*

- IEEE/CVF Winter Conference on Applications of Computer Vision*, pages 3209–3218, 2022. 5
- [28] S Alireza Golestaneh, Saba Dadsetan, and Kris M Kitani. No-reference image quality assessment via transformers, relative ranking, and self-consistency. In *Proceedings of the IEEE/CVF winter conference on applications of computer vision*, pages 1220–1230, 2022. 3
- [29] Sylvain Gugger, Lysandre Debut, Thomas Wolf, Philipp Schmid, Zachary Mueller, Sourab Mangrulkar, Marc Sun, and Benjamin Bossan. Accelerate: Training and inference at scale made simple, efficient and adaptable. <https://github.com/huggingface/accelerate>, 2022. 2
- [30] Jack Hessel, Ari Holtzman, Maxwell Forbes, Ronan Le Bras, and Yejin Choi. Clipscore: A reference-free evaluation metric for image captioning. In *Proceedings of the 2021 Conference on Empirical Methods in Natural Language Processing*, pages 7514–7528, 2021. 7
- [31] Martin Heusel, Hubert Ramsauer, Thomas Unterthiner, Bernhard Nessler, and Sepp Hochreiter. Gans trained by a two time-scale update rule converge to a local nash equilibrium. *NeurIPS*, 30, 2017. 6
- [32] Jonathan Ho, Ajay Jain, and Pieter Abbeel. Denoising diffusion probabilistic models. *arXiv preprint arxiv:2006.11239*, 2020. 4
- [33] Vlad Hosu, Hanhe Lin, Tamas Sziranyi, and Dietmar Saupe. Koniq-10k: An ecologically valid database for deep learning of blind image quality assessment. *IEEE Transactions on Image Processing*, 29:4041–4056, 2020. 3, 2
- [34] Edward J Hu, Yelong Shen, Phillip Wallis, Zeyuan Allen-Zhu, Yuanzhi Li, Shean Wang, Lu Wang, and Weizhu Chen. LoRA: Low-rank adaptation of large language models. In *ICLR*, 2022. 2
- [35] Gu Jinjin, Cai Haoming, Chen Haoyu, Ye Xiaoxing, Jimmy S Ren, and Dong Chao. Pipal: a large-scale image quality assessment dataset for perceptual image restoration. In *ECCV*, pages 633–651. Springer, 2020. 3, 2
- [36] Le Kang, Peng Ye, Yi Li, and David Doermann. Convolutional neural networks for no-reference image quality assessment. In *Proceedings of the IEEE conference on computer vision and pattern recognition*, pages 1733–1740, 2014. 3
- [37] Le Kang, Peng Ye, Yi Li, and David Doermann. Convolutional neural networks for no-reference image quality assessment. In *CVPR*, pages 1733–1740, 2014. 5
- [38] Sergey Kastrulin, Artem Konev, Alexander Shishenya, Eugene Lyapustin, Artem Khurshudov, Alexander Tselousov, Nikita Vinokurov, Denis Kuznedelev, Alexander Markovich, Grigoriy Livshits, et al. Yaart: Yet another art rendering technology. *arXiv preprint arXiv:2404.05666*, 2024. 2
- [39] Junjie Ke, Qifei Wang, Yilin Wang, Peyman Milanfar, and Feng Yang. Musiq: Multi-scale image quality transformer. In *ICCV*, pages 5148–5157, 2021. 5
- [40] Junjie Ke, Qifei Wang, Yilin Wang, Peyman Milanfar, and Feng Yang. Musiq: Multi-scale image quality transformer. In *Proceedings of the IEEE/CVF international conference on computer vision*, pages 5148–5157, 2021. 3
- [41] Yuval Kirstain, Adam Polyak, Uriel Singer, Shahbuland Matiana, Joe Penna, and Omer Levy. Pick-a-pic: An open dataset of user preferences for text-to-image generation. 2023. 1
- [42] Shu Kong, Xiaohui Shen, Zhe Lin, Radomir Mech, and Charless Fowlkes. Photo aesthetics ranking network with attributes and content adaptation. In *Computer Vision—ECCV 2016: 14th European Conference, Amsterdam, The Netherlands, October 11–14, 2016, Proceedings, Part I 14*, pages 662–679. Springer, 2016. 3
- [43] Black Forest Labs. Flux github repo. <https://github.com/black-forest-labs/flux>, 2024. 1, 2
- [44] Eric C Larson and Damon M Chandler. Most apparent distortion: full-reference image quality assessment and the role of strategy. *Journal of electronic imaging*, 19(1):011006–011006, 2010. 2
- [45] Xudong Li, Jingyuan Zheng, Runze Hu, Yan Zhang, Ke Li, Yunhang Shen, Xiawu Zheng, Yutao Liu, ShengChuan Zhang, Pingyang Dai, et al. Feature denoising diffusion model for blind image quality assessment. *arXiv preprint arXiv:2401.11949*, 2024. 1, 3
- [46] Zhi Li, Anne Aaron, Ioannis Katsavounidis, and Megha Manohara. Toward a practical perceptual video quality metric. URL: <https://netflixtechblog.com/toward-a-practical-perceptual-video-quality-metric-653f208b9652>, 2016. Date of access: 2024-05-01. 1
- [47] Hanhe Lin, Vlad Hosu, and Dietmar Saupe. Kadid-10k: A large-scale artificially distorted iqa database. In *2019 Eleventh International Conference on Quality of Multimedia Experience (QoMEX)*, pages 1–3. IEEE, 2019. 3, 2
- [48] Tsung-Yi Lin, Michael Maire, Serge Belongie, James Hays, Pietro Perona, Deva Ramanan, Piotr Dollár, and C Lawrence Zitnick. Microsoft coco: Common objects in context. In *ECCV*, pages 740–755. Springer, 2014. 6
- [49] Bingchen Liu, Ehsan Akhgari, Alexander Visheratin, Aleks Kamko, Linmiao Xu, Shivam Shrirao, Joao Souza, Suhail Doshi, and Daiqing Li. Playground v3: Improving text-to-image alignment with deep-fusion large language models. *arXiv preprint arXiv:2409.10695*, 2024. 2
- [50] Ilya Loshchilov and Frank Hutter. Decoupled weight decay regularization. <https://arxiv.org/abs/1711.05101>, 2019. 2
- [51] Ben Mildenhall, Pratul P. Srinivasan, Matthew Tancik, Jonathan T. Barron, Ravi Ramamoorthi, and Ren Ng. Nerf: representing scenes as neural radiance fields for view synthesis. *Commun. ACM*, 65(1):99–106, 2021. 10
- [52] Anish Mittal, Anush Krishna Moorthy, and Alan Conrad Bovik. No-reference image quality assessment in the spatial domain. *IEEE Transactions on image processing*, 21(12):4695–4708, 2012. 3
- [53] Anish Mittal, Rajiv Soundararajan, and Alan C Bovik. Making a “completely blind” image quality analyzer. *IEEE Signal processing letters*, 20(3):209–212, 2012.
- [54] Anush Krishna Moorthy and Alan Conrad Bovik. Blind image quality assessment: From natural scene statistics to perceptual quality. *IEEE transactions on Image Processing*, 20(12):3350–3364, 2011. 3
- [55] Chong Mou, Xintao Wang, Liangbin Xie, Yanze Wu, Jian Zhang, Zhongang Qi, and Ying Shan. T2i-adapter: Learning

- adapters to dig out more controllable ability for text-to-image diffusion models. In *AAAI*, pages 4296–4304, 2024. 2
- [56] Naila Murray, Luca Marchesotti, and Florent Perronnin. Ava: A large-scale database for aesthetic visual analysis. In *2012 IEEE conference on computer vision and pattern recognition*, pages 2408–2415. IEEE, 2012. 3, 2
- [57] A Deep Bilinear Convolutional Neural Network. Blind image quality assessment using a deep bilinear convolutional neural network. 3
- [58] Dustin Podell, Zion English, Kyle Lacey, Andreas Blattmann, Tim Dockhorn, Jonas Müller, Joe Penna, and Robin Rombach. Sdxl: Improving latent diffusion models for high-resolution image synthesis. In *ICLR*, 2024. 1, 3, 4
- [59] Adam Polyak, Amit Zohar, Andrew Brown, Andros Tjandra, Animesh Sinha, Ann Lee, Apoorv Vyas, Bowen Shi, Chih-Yao Ma, Ching-Yao Chuang, et al. Movie gen: A cast of media foundation models. *arXiv preprint arXiv:2410.13720*, 2024. 3
- [60] Ekta Prashnani, Hong Cai, Yasamin Mostofi, and Pradeep Sen. Pieapp: Perceptual image-error assessment through pairwise preference. In *CVPR*, 2018. 6
- [61] Aditya Ramesh, Mikhail Pavlov, Gabriel Goh, Scott Gray, Chelsea Voss, Alec Radford, Mark Chen, and Ilya Sutskever. Zero-shot text-to-image generation. In *International conference on machine learning*, pages 8821–8831. Pmlr, 2021. 2
- [62] Robin Rombach, Andreas Blattmann, Dominik Lorenz, Patrick Esser, and Björn Ommer. High-resolution image synthesis with latent diffusion models. In *Proceedings of the IEEE/CVF conference on computer vision and pattern recognition*, pages 10684–10695, 2022. 2, 10
- [63] Nataniel Ruiz, Yuanzhen Li, Varun Jampani, Yael Pritch, Michael Rubinstein, and Kfir Aberman. Dreambooth: Fine tuning text-to-image diffusion models for subject-driven generation. In *CVPR*, pages 22500–22510, 2023. 2
- [64] Chitwan Saharia, William Chan, Saurabh Saxena, Lala Li, Jay Whang, Emily L Denton, Kamyar Ghasemipour, Raphael Gontijo Lopes, Burcu Karagol Ayan, Tim Salimans, et al. Photorealistic text-to-image diffusion models with deep language understanding. *Advances in neural information processing systems*, 35:36479–36494, 2022. 2
- [65] Tim Salimans, Ian Goodfellow, Wojciech Zaremba, Vicki Cheung, Alec Radford, and Xi Chen. Improved techniques for training gans. *NeurIPS*, 29, 2016. 7
- [66] Gustavo Santana. Dataset of user-generated prompts collected from lexicart website. date of access: November 14, 2024. 5
- [67] Christoph Schuhmann. Laion aesthetics predictor, 2023. date of access: November 14, 2024. 2
- [68] Christoph Schuhmann, Romain Beaumont, Richard Vencu, Cade Gordon, Ross Wightman, Mehdi Cherti, Theo Coombes, Aarush Katta, Clayton Mullis, Mitchell Wortsman, Patrick Schramowski, Srivatsa Kundurthy, Katherine Crowson, Ludwig Schmidt, Robert Kaczmarczyk, and Jenia Jitsev. Laion-5b: an open large-scale dataset for training next generation image-text models. Red Hook, NY, USA, 2024. Curran Associates Inc. 5
- [69] Piyush Sharma, Nan Ding, Sebastian Goodman, and Radu Soricut. Conceptual captions: A cleaned, hypernymed, image alt-text dataset for automatic image captioning. In *Proceedings of ACL*, 2018. 5
- [70] Hamid R Sheikh and Alan C Bovik. A visual information fidelity approach to video quality assessment. In *The first international workshop on video processing and quality metrics for consumer electronics*, pages 2117–2128. sn, 2005. 3
- [71] Hamid R Sheikh, Muhammad F Sabir, and Alan C Bovik. A statistical evaluation of recent full reference image quality assessment algorithms. *IEEE Transactions on image processing*, 15(11):3440–3451, 2006. 2
- [72] Maksim Siniukov, Anastasia Antsiferova, Dmitriy Kulikov, and Dmitriy Vatolin. Hacking vmaf and vmaf neg: Vulnerability to different preprocessing methods. In *Proceedings of the 2021 4th Artificial Intelligence and Cloud Computing Conference*, page 89–96, New York, NY, USA, 2022. Association for Computing Machinery. 1
- [73] Jianlin Su, Murtadha Ahmed, Yu Lu, Shengfeng Pan, Wen Bo, and Yunfeng Liu. Roformer: Enhanced transformer with rotary position embedding. *Neurocomput.*, 568(C), 2024. 11
- [74] Shaolin Su, Qingsen Yan, Yu Zhu, Cheng Zhang, Xin Ge, Jinqui Sun, and Yanning Zhang. Blindly assess image quality in the wild guided by a self-adaptive hyper network. In *CVPR*, 2020. 5
- [75] Shaolin Su, Qingsen Yan, Yu Zhu, Cheng Zhang, Xin Ge, Jinqui Sun, and Yanning Zhang. Blindly assess image quality in the wild guided by a self-adaptive hyper network. In *Proceedings of the IEEE/CVF conference on computer vision and pattern recognition*, pages 3667–3676, 2020. 3
- [76] Hossein Talebi and Peyman Milanfar. Nima: Neural image assessment. *IEEE transactions on image processing*, 27(8): 3998–4011, 2018. 3
- [77] Hossein Talebi and Peyman Milanfar. Nima: Neural image assessment. *IEEE transactions on image processing*, 27(8): 3998–4011, 2018. 5
- [78] Jianyi Wang, Kelvin CK Chan, and Chen Change Loy. Exploring clip for assessing the look and feel of images. In *Proceedings of the AAAI Conference on Artificial Intelligence*, pages 2555–2563, 2023. 3, 5
- [79] Zhou Wang, Eero P Simoncelli, and Alan C Bovik. Multiscale structural similarity for image quality assessment. In *The Thirty-Seventh Asilomar Conference on Signals, Systems & Computers*, 2003, pages 1398–1402. Ieee, 2003. 3
- [80] Zhou Wang, Alan C Bovik, Hamid R Sheikh, and Eero P Simoncelli. Image quality assessment: from error visibility to structural similarity. *IEEE transactions on image processing*, 13(4):600–612, 2004. 3, 6
- [81] Zhaoyang Wang, Bo Hu, Mingyang Zhang, Jie Li, Leida Li, Maoguo Gong, and Xinbo Gao. Diffusion model based visual compensation guidance and visual difference analysis for no-reference image quality assessment. *arXiv preprint arXiv:2402.14401*, 2024. 1, 3
- [82] Xiaoshi Wu, Keqiang Sun, Feng Zhu, Rui Zhao, and Hongsheng Li. Better aligning text-to-image models with human preference, 2023. 1

- [83] S Xiao, Y Wang, J Zhou, H Yuan, X Xing, and R Yan. Omnigen: Unified image generation. *arXiv preprint arXiv:2409.11340*, 2024. [1](#)
- [84] xiaoju ye. calfllops: a flops and params calculate tool for neural networks in pytorch framework, 2023. [1](#)
- [85] Jiazheng Xu, Xiao Liu, Yuchen Wu, Yuxuan Tong, Qinkai Li, Ming Ding, Jie Tang, and Yuxiao Dong. Imagereward: Learning and evaluating human preferences for text-to-image generation. *NeurIPS*, 36, 2024. [1](#)
- [86] Sidi Yang, Tianhe Wu, Shuwei Shi, Shanshan Lao, Yuan Gong, Mingdeng Cao, Jiahao Wang, and Yujiu Yang. Maniqa: Multi-dimension attention network for no-reference image quality assessment. In *CVPR*, pages 1191–1200, 2022. [3](#), [5](#)
- [87] Hu Ye, Jun Zhang, Sibao Liu, Xiao Han, and Wei Yang. Ip-adapter: Text compatible image prompt adapter for text-to-image diffusion models. *arXiv preprint arxiv:2308.06721*, 2023. [1](#), [2](#), [3](#)
- [88] Zhenqiang Ying, Haoran Niu, Praful Gupta, Dhruv Mahajan, Deepti Ghadiyaram, and Alan Bovik. From patches to pictures (paq-2-piq): Mapping the perceptual space of picture quality. In *Proceedings of the IEEE/CVF conference on computer vision and pattern recognition*, pages 3575–3585, 2020. [3](#), [2](#)
- [89] Jiahui Yu, Yuanzhong Xu, Jing Yu Koh, Thang Luong, Gungjan Baid, Zirui Wang, Vijay Vasudevan, Alexander Ku, Yinfei Yang, Burcu Karagol Ayan, Ben Hutchinson, Wei Han, Zarana Parekh, Xin Li, Han Zhang, Jason Baldridge, and Yonghui Wu. Scaling autoregressive models for content-rich text-to-image generation. *Transactions on Machine Learning Research*, 2022. Featured Certification. [5](#), [2](#)
- [90] Lin Zhang, Lei Zhang, and Alan C Bovik. A feature-enriched completely blind image quality evaluator. *IEEE Transactions on Image Processing*, 24(8):2579–2591, 2015. [3](#)
- [91] Lvmin Zhang, Anyi Rao, and Maneesh Agrawala. Adding conditional control to text-to-image diffusion models. In *ICCV*, 2023. [1](#), [2](#)
- [92] Richard Zhang, Phillip Isola, Alexei A Efros, Eli Shechtman, and Oliver Wang. The unreasonable effectiveness of deep features as a perceptual metric. In *CVPR*, 2018. [6](#)
- [93] Weixia Zhang, Kede Ma, Jia Yan, Dexiang Deng, and Zhou Wang. Blind image quality assessment using a deep bilinear convolutional neural network. *IEEE Transactions on Circuits and Systems for Video Technology*, 30(1):36–47, 2020. [5](#)
- [94] Weixia Zhang, Guangtao Zhai, Ying Wei, Xiaokang Yang, and Kede Ma. Blind image quality assessment via vision-language correspondence: A multitask learning perspective. In *Proceedings of the IEEE/CVF conference on computer vision and pattern recognition*, pages 14071–14081, 2023. [3](#)
- [95] Weixia Zhang, Guangtao Zhai, Ying Wei, Xiaokang Yang, and Kede Ma. Blind image quality assessment via vision-language correspondence: A multitask learning perspective. In *IEEE/CVF Conference on Computer Vision and Pattern Recognition*, page 14071–14081, 2023. [5](#)
- [96] Anastasia V. Zvezdakova, Sergey Zvezdakov, Dmitriy L. Kulikov, and Dmitriy Sergeevich Vatolin. Hacking vmaf with video color and contrast distortion. *GraphiCon'2019 Proceedings. Volume 2*, 2019. [1](#)



# IQA-Adapter: Exploring Knowledge Transfer from Image Quality Assessment to Diffusion-based Generative Models

## Supplementary Material

### 7. Employed IQA/IAA methods

Table 2 provides a detailed summary of all IQA/IAA methods used in this study, along with their training datasets and architectural details. The column "PyIQA" lists model identifiers from the PyIQA library [9]. The column "Task" specifies supported tasks: most models are designed for IQA, while some (e.g., TOPIQ, MUSIQ) support both IQA and IAA, and others (e.g., NIMA) are exclusive to IAA. The column "Datasets" lists the datasets associated with each model; note that the models were not trained on mixtures of datasets, except for LIQE-MIX, which was specifically trained on a dataset mixture. For models like TOPIQ, there are several variants, each trained on a distinct dataset. The column "Arch" outlines the backbone architecture of the models. Most models are trained using finetuning of a pretrained model; however, some, like MUSIQ, are trained from scratch. The final three columns, "Params," "FLOPs," and "MACs," highlight the performance metrics of the models. FLOPs and MACs were computed using the callops package [84].

Table 3 provides a detailed overview of the datasets used for training the IQA and IAA models. The column "Type" categorizes the datasets: FR indicates the presence of a distortion-free reference image used for collecting subjective scores, whereas NR denotes datasets without such references. The column "Year" indicates the release year of each dataset. The column "# Ref" specifies the number of reference images used to generate distorted samples through augmentations. The column "# Dist" represents the total number of samples in the dataset. The column "Dist Type" describes how distorted images were created: "synthetic" refers to distortions introduced via augmentations such as JPEG compression or blurring, "algorithmic" applies to distortions generated by neural networks, such as GAN-based modifications, "authentic" denotes images captured in natural, real-world conditions, and "aesthetics" refers to high-quality images sourced from stock photography collections. The column "# Rating" indicates the number of ratings collected via crowdsourcing platforms. The column "Original size" details the resolution of images within the datasets.

### 8. Negative Guidance

Since the concept of visual quality has clearly defined notions of "good" and "bad," it becomes feasible to apply **negative guidance**, akin to its application in text-based generation. Negative guidance for text involves using an additional

text prompt that is semantically opposite to the desired outcome. This serves as a conditioning factor in the unconditional part of the generation process:

$$\hat{\epsilon}_\theta(z_t|c_t, q) = \epsilon_\theta(z_t|\emptyset) + g \cdot (\epsilon_\theta(z_t|c_t, q) - \epsilon_\theta(z_t|\emptyset))$$

where  $\epsilon_\theta$  is a latent diffusion model,  $g$  is guidance scale,  $c_t$  is a textual condition,  $q$  is desired quality of image and  $\emptyset$  is an empty condition.

This approach pushes the latent representation of the generated image away from producing undesired features described in the negative prompt.

The standard method for using an IP-Adapter assumes a null-condition in the unconditional part of the noise prediction, as there is no explicit counter-concept for an image prompt. The task of quality conditioning, however, enables defining negative guidance as:

$$\hat{\epsilon}_\theta(z_t|c_t, q) = \epsilon_\theta(z_t|c_t^{\text{neg}}, q^{\text{neg}}) + g \cdot (\epsilon_\theta(z_t|c_t, q) - \epsilon_\theta(z_t|c_t^{\text{neg}}, q^{\text{neg}}))$$

where  $q^{\text{neg}}$  specifies a quality level opposite to the desired one and  $c_t^{\text{neg}}$  is negative prompt. Since the input scores are normalized with a mean of 0, we can set  $q^{\text{neg}} = -q$ .

Using this approach enhances the adapter's effect, even with moderate adapter strengths. The resulting images become more vivid, sharp, and, in a sense, stylized to align with the ideals of the target metric. Examples of applying negative guidance with various types of negative conditions are presented in Figure 6.

Strong negative guidance significantly improves metric scores, with generalization across different metrics. Figure 8 shows average improvements increasing from 5-6% to 8-10% relative to the base model. However, strong negative guidance with high adapter scales can result in overly clean, saturated, sharp images, losing fine details (Figure 7). This effect intensifies with higher scales.

These findings emphasize the need for subjective validation, as IQA/IAA models may have biases or vulnerabilities, especially in adversarial scenarios. The generalization of quality improvements suggests shared biases among models, similar to vulnerabilities identified in the VMAF IQA metric [46, 72, 96].

### 9. IQA-Adapter training

The IQA-Adapters were trained on the CC3M dataset, which consists of approximately 3 million text-image pairs,

Model	PyIQA	Task	Datasets	Arch	Params	FLOPS	MACs
TOPIQ	topiq_nr	IQA / IAA	KonIQ-10k [33], SPAQ [20], FLIVE [88], AVA [56]	ResNet50	45.2M	886 GFLOPS	441.5 GMACs
DBCNN	dbcnn	IQA	KonIQ-10k [33]	VGG16	15.3M	2.1 TFLOPS	1 TMACs
HyperIQA	hyper_iqa	IQA	KonIQ-10k [33]	ResNet50	27.4M	2.6 TFLOPS	1.3 TMACs
ARNIQA	arniqa	IQA	KonIQ-10 [33], FLIVE [88], KADID [47]	ResNet50	23.5M	-	-
LIQE-Mix	liqe_mix	IQA	Mixed (LIVE [71], CSIQ [44], KADID [47], CLIVE [24], BID [13], KonIQ-10k [33])	OpenAI CLIP ViT-B/32	151.3M	1.7 TFLOPS	850.7 GMACs
MANIQA	maniqa	IQA	KonIQ-10k [33], PIPAL [35]	ViT-B/8	135.7M	56.4 TFLOPS	28.2 TMACs
CNN-IQA	cnniqa	IQA	KonIQ-10k [33]	CNN	729.8K	49.4 GFLOPS	24.5 GMACs
LIQE	liqe	IQA	KonIQ-10k [33]	OpenAI CLIP ViT-B/32	151.3M	1.7 TFLOPS	850.7 GMACs
MUSIQ	musiq	IQA / IAA	KonIQ-10k [33], AVA [56], FLIVE [88]	Multiscale ViT	27.1M	400.6 GFLOPS	199.1 GMACs
CLIP-IQA+	cliq_iqa+	IQA	KonIQ-10k [33]	OpenAI CLIP ResNet50	102.0M	981.1 GFLOPS	489.2 GMACs
NIMA	nima	IAA	AVA [56]	InceptionResnetV2	54.3M	342.9 GFLOPS	171 GMACs
LAION-Aes	laion_aes	IAA	Other	OpenAI CLIP ViT-L14	428.5M	2 TFLOPS	1 TMACs
TReS	tres	IQA	FLIVE [88]	ResNet50	152.5M	25.9 TFLOPS	12.9 TMACs

Table 2. List of employed metrics with their corresponding training datasets.

Type	Dataset	Year	# Ref	# Dist	Dist Type.	# Rating	Original size $W \times H$
FR	LIVE [71]	2006	29	779	Synthetic	25k	$768 \times 512$ (typical)
	CSIQ [44]	2010	30	866	Synthetic	5k	$512 \times 512$
	KADID-10k [47]	2019	81	10.1k	Synthetic	30.4k	$512 \times 384$
	PIPAL [35]	2020	250	29k	Syth.+alg.	1.13M	$288 \times 288$
NR	BID [13]	2010	120	6000	Synthetic	$\sim 7k$	1K – 2K
	AVA [56]	2012	-	250k	Aesthetic	53M	$< 800$
	CLIVE [24]	2015	-	1.2k	Authentic	350k	$500 \times 500$
	KonIQ-10k [33]	2018	-	10k	Authentic	1.2M	$512 \times 384$
	SPAQ [20]	2020	-	11k	Authentic	-	4K (typical)
	FLIVE [88]	2020	-	160k	Auth.+Aest.	3.9M	Train $< 640$   Test $> 640$

Table 3. Description of training datasets from Table 2.

for 24,000 steps, followed by fine-tuning on a subset of the LAION-5B dataset, containing 170,000 images, for 3,000 steps. During training on CC3M, the images were center-cropped to a resolution of  $512 \times 512$ . For fine-tuning on LAION, the resolution was increased to  $1024 \times 1024$  to match SDXL’s native resolution. We used the AdamW [50] optimizer with  $\beta_1 = 0.9$ ,  $\beta_2 = 0.999$  and a weight decay of  $1 \times 10^{-2}$  for the IQA-Adapter parameters. All experiments utilized bf16 mixed precision to improve computational efficiency. Multi-node training was conducted using the accelerate [29] library, enabling efficient scaling across our hardware setup. The learning rate was set to  $10^{-4}$  during the primary training phase on CC3M and reduced to  $10^{-5}$  for the fine-tuning on the LAION subset.

To ensure consistency and reproducibility, all experiments were conducted within Docker containers built from a shared image. The environment included Python 3.11, PyTorch 2.1, and other dependencies required for training.

## 10. High-quality conditioning: more results

### 10.1. Gradient-based guidance

Figure 9(b) presents the relative gain in metric scores when using the gradient-based approach to optimize image qual-

ity during generation for prompts from PartiPrompts [89]. Unlike IQA-Adapter, direct optimization of the target metric improves that specific metric alone, while most other quality metrics tend to decline. This observation highlights the adversarial nature of gradient-based guidance, further confirmed by a closer examination of changes in generated images, which reveal adversarial patterns (as shown in Figure 20). Interestingly, certain metrics, such as ARNIQA (trained on KADID), LAION-AES, and LIQE MIX, show improvements even when unrelated quality metrics are targeted for optimization. This behavior points to their inherent instability and susceptibility to adversarial attacks, raising questions about their robustness as quality measures.

### 10.2. IQA-Adapter

Figure 9(a) provides additional results of high-quality conditioning with IQA-Adapter on PartiPrompts. The results on this dataset mirror the trends observed on the Lexica.art prompts, discussed in Section 4.2. Specifically, conditioning on the 99th percentile of target metrics not only boosts the target metrics themselves but also improves most other metrics, highlighting the strong transferability of IQA-Adapter. However, the average metric improvements on PartiPrompts are 1–2% lower than those observed on

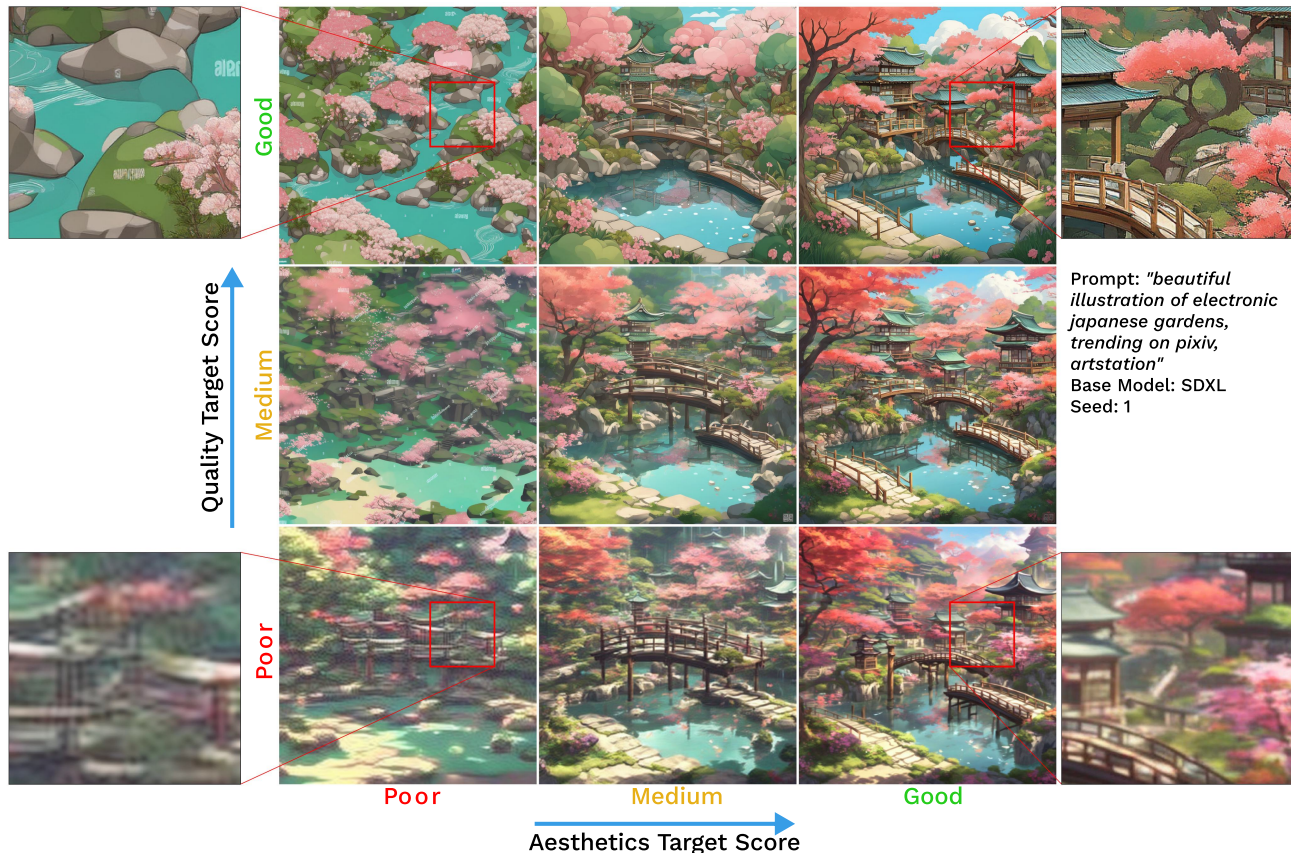


Figure 6. Quality-aware image generation using IQA-Adapter combined with negative guidance. Compared to Figure 1, negative guidance exhibits stronger effect.

Lexica.art. This discrepancy can likely be attributed to the quality and completeness of the prompts. Unlike the more detailed and descriptive prompts in Lexica.art, PartiPrompts consists of shorter and more generic prompts. These simpler prompts impose fewer demands on the generation process, limiting the need for detailed generation, which is one of a key factors behind the significant metric improvements achieved by IQA-Adapter on Lexica.art.

## 11. Evaluating Generative Capabilities: more results

Table 4 provides the complete results on the GenEval benchmark. Among the 25 evaluated IQA-Adapters, five outperform the Base Model in terms of the overall score. Notably, even the weakest IQA-Adapter surpasses the Base Model in the Counting and Position metrics. However, the best-performing IQA-Adapter underperforms the Base Model in the Two Object, Colors, and Single Object metrics. Overall, while all IQA-Adapters achieve performance levels comparable to the initial model, some manage to outperform it in specific areas.

Table 5 presents quantitative results for the FID, IS, and CLIP-similarity metrics. With a few exceptions, most IQA-Adapters exhibit slightly higher FID scores on the full MS COCO training dataset compared to the Base Model. This can be attributed to the diverse quality distribution of the dataset, which contains images of varying visual fidelity. Since IQA-Adapters are conditioned to prioritize high-quality generation, they naturally shift the output distribution toward a more specific subdomain characterized by higher visual quality. As a result, the distance to the broader, more heterogeneous image distribution of the full dataset increases. To address this domain shift, we also calculate FID scores on high-quality subsets of the MS COCO training dataset. These subsets include the top 10% and 25% of images, selected based on average quality scores from multiple IQA and IAA models. In this scenario, most IQA-Adapters consistently achieve lower FID scores than the Base Model, demonstrating superior alignment with the high-quality subsets.

In addition to FID, we evaluate the Inception Score (IS) and CLIP-similarity metrics. CLIP-Text (CLIP-T) measures the similarity between generated images and their cor-



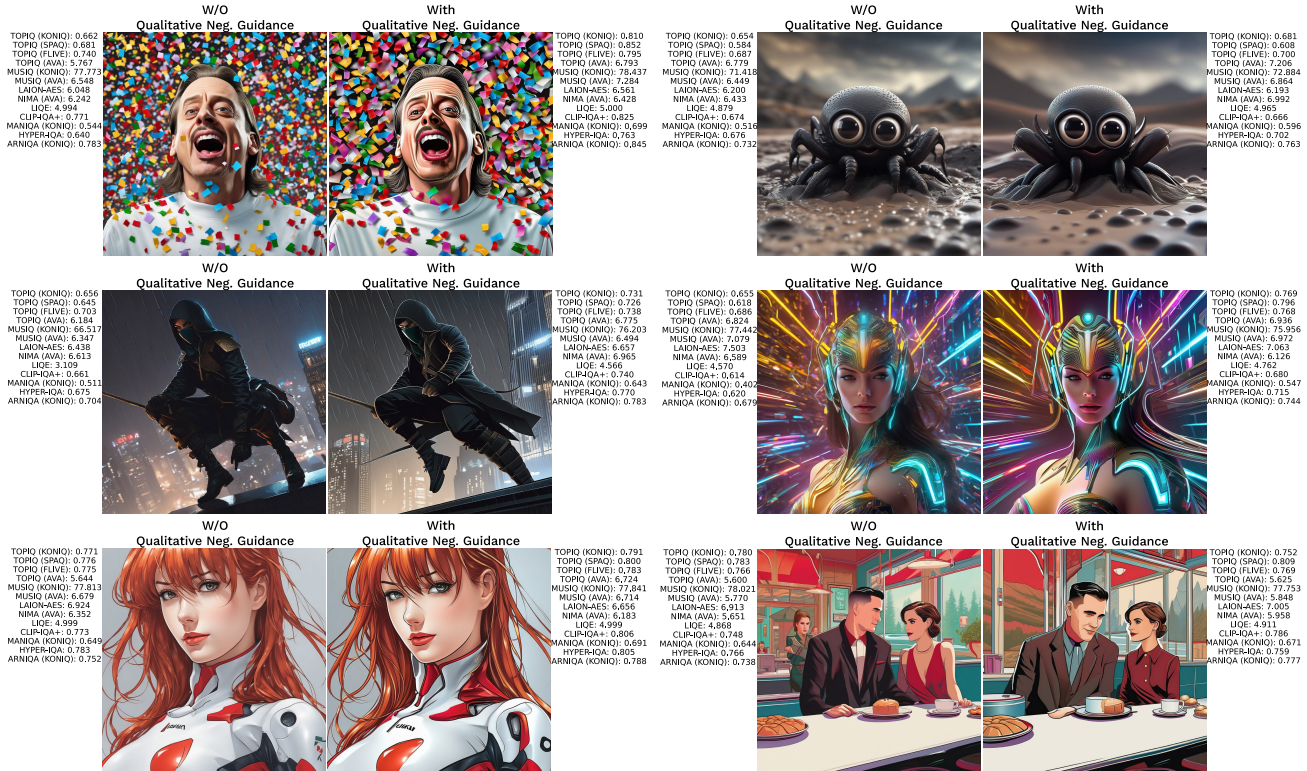


Figure 7. Example of images generated with and without negative guidance. Negative guidance magnifies the impact of the IQA-Adapter and often results in the “stylisation” effect that is highly rated by most IQA/IAA models.

IQA/IAA Models used in IQA-Adapter	IQA														IAA				VLM-based				Mean (Overall)
	ARNIQA (KADID)	TOPIO (KONID)	MANIQA (KONID)	ARNIQA (KONID)	MUSIO (KONID)	HYPER-IQA	CNNIQA -	DBCCNN	MANIQA (PIPAL)	TOPIO (SPAQ)	MUSIO (FLIVE)	TOPIO (FLIVE)	TRES (FLIVE)	ARNIQA (FLIVE)	MUSIO (AWA)	NMA (AWA)	TOPIO (IAB)	LAIQN-AES	LIQE-MIX	LIQE-MIX	LIQE-MIX	LIQE-MIX	
TOPIO, LAION-AES	-10.9	12.9	34.7	15.3	5.3	17.6	0.2	13.1	13.8	22.1	3.4	5.0	5.0	9.9	3.8	5.2	3.9	-1.9	17.8	5.9	19.4	10.6	
4xTOPIO (MultiDataset)	-1.0	13.4	33.3	14.5	4.9	20.5	0.8	12.7	13.1	22.4	3.5	5.3	5.0	8.6	6.2	6.9	7.1	-1.9	16.3	5.1	18.4	10.2	
TOPIO (KONIO)	-2.2	13.3	30.1	11.1	4.2	17.4	1.0	12.1	13.6	20.6	3.4	4.5	4.7	7.9	1.7	1.5	1.8	-0.8	12.7	4.8	17.4	8.8	
HYPER-IQA	-0.8	13.1	28.2	10.2	4.5	18.2	1.8	12.0	12.0	18.8	3.1	3.9	3.9	6.4	1.7	1.2	0.7	0.3	12.9	4.7	17.4	8.3	
3xARNIQA, LIQE-MIX (MultiDataset)	18.5	10.6	22.9	9.5	4.2	12.9	1.4	9.6	8.1	15.9	3.3	4.0	3.8	6.4	2.5	2.3	1.9	-1.2	12.2	5.9	17.0	8.2	
TOPIO (SPAQ)	-2.8	10.4	29.5	10.6	4.0	16.6	1.3	10.0	10.9	20.8	3.1	4.1	4.3	6.8	3.1	2.5	2.5	-1.2	11.9	4.6	16.2	8.1	
DBCCNN	-3.3	10.4	28.4	9.1	4.2	16.9	1.1	11.4	11.8	20.1	3.1	3.7	3.8	6.0	4.2	3.0	2.8	-0.9	13.5	3.8	15.0	8.0	
ARNIQA (KONIO)	0.1	12.4	27.1	10.5	4.2	16.1	1.5	10.9	10.1	17.6	3.1	3.8	3.9	7.1	0.3	-0.1	-0.4	-1.4	12.8	5.2	17.1	7.7	
MUSIO (AWA)	-5.0	9.9	23.8	10.9	3.3	12.9	1.1	9.3	9.3	12.7	2.3	3.5	4.0	6.2	4.4	5.2	4.9	-0.4	10.8	3.6	14.6	7.5	
MANIQA (KONIO)	-5.7	8.3	23.2	8.1	3.9	11.6	0.7	8.6	11.9	15.5	3.1	3.8	3.9	7.1	0.4	2.8	1.7	-1.0	13.5	5.4	14.4	7.3	
TRES (FLIVE)	-1.4	9.1	21.3	7.9	4.3	12.1	2.2	8.7	5.8	15.9	3.4	4.0	4.5	6.1	2.3	2.2	1.5	-1.3	10.2	4.1	15.1	6.7	
ARNIQA (FLIVE)	-3.8	8.5	22.4	8.1	4.1	11.1	1.8	8.1	7.1	16.7	3.4	3.6	4.1	6.4	0.5	0.6	-0.2	-1.3	10.1	4.2	14.8	6.6	
MANIQA (PIPAL)	-7.8	7.8	20.6	6.9	3.2	9.4	0.1	7.2	12.1	14.0	2.7	3.6	3.7	5.8	-0.9	1.5	1.3	-1.7	12.0	5.3	15.3	6.6	
CNNIQA -	-2.6	9.6	22.1	8.1	3.4	13.7	0.8	9.3	9.3	16.2	2.8	3.6	3.8	6.3	-0.5	0.9	0.6	-0.7	10.0	4.3	14.6	6.5	
LIQE	-1.2	10.2	18.9	8.1	3.9	11.6	1.6	8.6	7.3	12.2	2.5	3.3	3.0	4.8	0.8	2.2	1.5	-1.2	10.2	4.9	16.2	6.3	
TOPIO (IAB)	-8.7	9.4	15.3	9.9	3.4	9.3	1.5	7.9	5.7	7.3	1.3	2.7	2.7	4.4	5.5	6.3	6.1	-1.1	8.3	3.3	13.1	6.2	
NMA (AWA)	11.4	7.2	16.0	8.3	3.0	8.2	1.2	6.7	6.1	9.6	1.8	2.8	2.8	4.9	4.0	6.6	5.4	-0.9	7.5	3.4	12.5	6.1	
TOPIO (FLIVE)	-7.1	8.7	15.7	6.8	4.2	9.0	1.7	7.9	6.5	13.1	3.0	3.8	3.6	5.0	0.9	2.5	1.1	-0.9	9.1	4.2	14.5	6.1	
MUSIO (KONIO)	-6.9	6.9	17.3	7.3	4.0	9.2	0.7	7.0	7.9	11.0	2.8	3.3	3.4	5.3	-1.0	1.7	0.9	-1.6	9.6	5.3	13.9	5.8	
CLIP-IQA+ - LIQE-MIX	-3.7	6.6	18.5	5.9	3.7	8.7	1.2	7.0	6.1	12.4	2.7	3.2	2.9	4.4	1.0	2.2	1.1	-1.5	12.4	5.2	13.7	5.8	
CLIP-IQA+	10.1	4.3	11.9	5.9	3.5	4.4	0.5	3.9	5.4	8.0	2.4	3.2	2.7	4.8	-0.1	3.7	2.5	-1.8	12.8	5.3	14.2	5.1	
MUSIO (FLIVE)	-2.5	6.9	17.8	5.9	3.9	9.0	1.6	6.5	4.8	13.2	3.2	3.4	3.3	4.8	0.2	1.6	-0.2	-2.0	8.7	3.5	12.4	5.1	
LIQE-MIX	-0.4	4.5	13.0	5.1	3.2	7.0	1.1	5.2	5.4	8.7	2.2	2.6	2.6	3.3	-0.8	1.2	0.8	-1.5	7.3	5.1	10.8	4.2	
ARNIQA (KADID)	9.7	3.0	9.9	4.9	3.0	4.0	1.0	3.5	2.1	5.9	1.9	2.2	1.9	2.7	-0.5	1.6	0.8	-1.4	6.3	4.8	10.5	3.7	

Evaluation Quality Metric

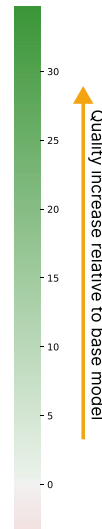


Figure 8. Results of high-quality conditioning for different IQA-Adapters with strong **negative guidance** on user-generated prompts from Lexica.art website (similarly to the Figure 3 from the main document). We use  $P_{99\%}$  (99-th percentile) for positive quality-condition and  $-1 \cdot P_{99\%}$  for negative one.



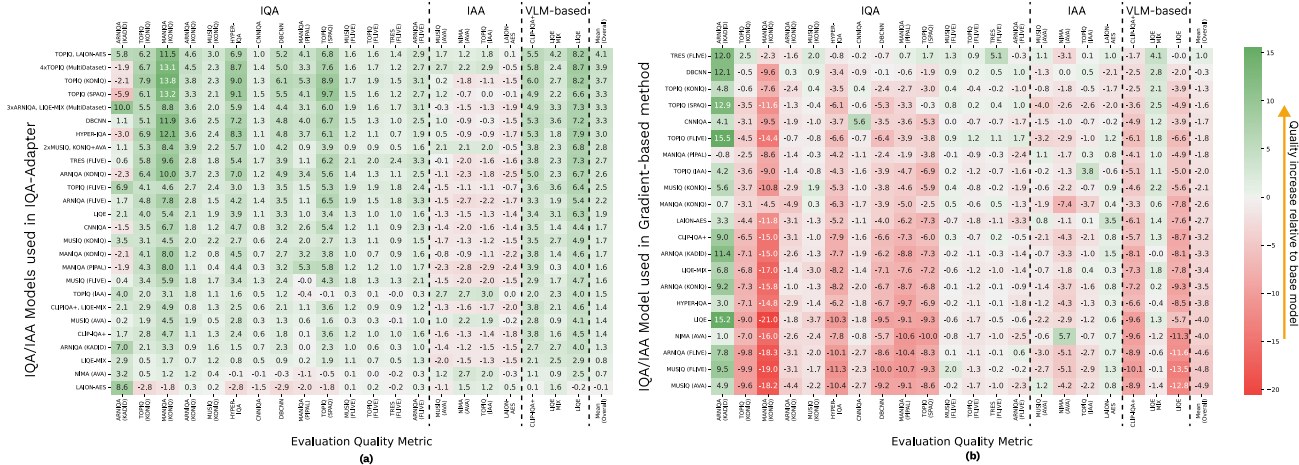


Figure 9. Quality improvement relative to base model (in %) for the IQA-Adapters trained on different IQA/IAA models (a) and gradient-based method targeted on different IQA/IAA models (b). All IQA-Adapters are conditioned with high target quality (99th percentile of the training dataset) and use the same prompts and seeds. Prompts are taken from PartiPrompts.

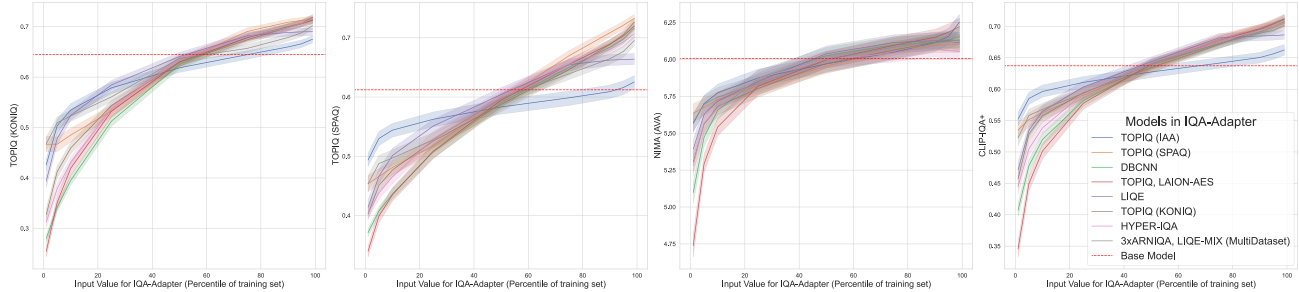


Figure 10. The relationship between input quality-condition (represented as a percentile of target IQA/IAA model on the training dataset) and image-quality scores evaluated by four different metrics (TOPIQ (KonIQ), TOPIQ (SPAQ), CLIP-IQA+, LIQE).

responding text prompts, using COCO captions as prompts in our experiment. CLIP-Image (CLIP-I) measures the distance between generated images and the real images corresponding to the captions. Results indicate that most IQA-Adapters achieve better CLIP scores than the Base Model, highlighting improved prompt-following capabilities. However, the Inception Score results are slightly lower compared to the Base Model. It is worth noting that the IS differences fall within the confidence interval. Additionally, IS is not well-suited for evaluating SDXL model, which is trained on large-scale internet datasets [7]. Furthermore, as IQA-Adapters generate more complex and detailed images, the classifier behind Inception Score struggles to identify the main object within the scene, further complicating its evaluation.

## 12. Alignment with qualitative condition: more results

To further evaluate the relationship between the input quality conditions provided to the IQA-Adapter during image

generation and the quality of the resulting images, we analyzed correlations between the target quality and various metric scores. Figure 16 shows estimated correlations for each trained IQA-Adapter. Generally, the metrics demonstrate a strong alignment with the target quality, with the highest correlations observed when comparing different IQA models. In contrast, weaker correlations are noted when IQA models are compared with IAA models. Among the evaluated metrics, the poorest correlations are associated with images generated using the IQA-Adapter based on the IAA metric, LAION-Aes. Interestingly, even the metric's own values fail to exhibit significant correlation, which may be attributed to the IQA-Adapter training process, specifically the additional fine-tuning step. However, when LAION-Aes is paired with an IQA metric, the correlations with IAA models improves significantly. For example, the IQA-Adapter trained on the TOPIQ and LAION-Aes metrics achieves high correlations with both IQA and IAA models, making it an optimal choice for generating images with high visual quality.

Models in IQA-Adapter	Two Object <sup>↑</sup>	Attribute Binding <sup>↑</sup>	Colors <sup>↑</sup>	Counting <sup>↑</sup>	Single Object <sup>↑</sup>	Position <sup>↑</sup>	Overall <sup>↑</sup>
LAION-AES	65.40%	16.75%	84.57%	45.00%	97.50%	12.25%	53.58%
MANIQA (PIPAL)	73.23%	20.25%	86.17%	36.56%	96.56%	10.50%	53.88%
ARNIQA (FLIVE)	69.70%	18.50%	84.04%	42.50%	97.81%	12.25%	54.13%
TOPIQ (KONIQ)	71.97%	18.75%	85.11%	38.75%	98.12%	13.75%	54.41%
CLIQQA+, LIQE-MIX	71.72%	20.25%	85.64%	41.25%	97.81%	11.75%	54.74%
LIQE-MIX	68.43%	19.50%	87.50%	43.12%	98.12%	12.75%	54.91%
MUSIQ (FLIVE)	69.19%	23.25%	<u>88.30%</u>	39.38%	99.06%	12.50%	55.28%
4xTOPIQ (MultiDataset)	72.47%	21.75%	87.77%	40.31%	97.19%	12.25%	55.29%
TOPIQ, LAION-AES	69.70%	18.75%	85.90%	45.31%	<u>99.38%</u>	13.00%	55.34%
CNNIQA	71.72%	19.50%	87.50%	41.56%	98.12%	<u>14.25%</u>	55.44%
MUSIQ (AVA)	69.44%	<u>24.25%</u>	86.97%	40.94%	99.06%	12.50%	55.53%
2xMUSIQ, KONIQ+AVA	73.23%	22.75%	86.44%	40.94%	98.12%	12.50%	55.66%
TOPIQ (SPAQ)	73.48%	21.25%	86.70%	43.75%	97.50%	12.50%	55.86%
3xARNIQA, LIQE-MIX (MultiDataset)	<u>73.99%</u>	19.25%	<b>89.36%</b>	39.69%	<b>99.69%</b>	13.75%	55.95%
MANIQA (KONIQ)	73.48%	<b>25.75%</b>	<u>88.30%</u>	38.75%	96.88%	12.75%	55.98%
LIQE	72.73%	21.75%	<u>86.97%</u>	41.56%	98.75%	<u>14.25%</u>	56.00%
NIMA (AVA)	70.96%	23.00%	87.50%	44.69%	98.44%	11.50%	56.01%
MUSIQ (KONIQ)	73.74%	21.00%	86.44%	<b>46.25%</b>	97.50%	11.50%	56.07%
ARNIQA (KONIQ)	71.97%	22.00%	87.50%	44.38%	98.12%	12.75%	56.12%
CLIP-IQA+	72.73%	22.75%	88.03%	43.44%	98.44%	12.25%	56.27%
HYPER-IQA	<u>73.99%</u>	<u>25.25%</u>	85.90%	39.69%	98.75%	<b>14.75%</b>	56.39%
DBCNN	73.48%	22.75%	86.44%	44.38%	99.06%	13.00%	56.52%
ARNIQA (KADID)	72.98%	23.25%	86.97%	<u>45.94%</u>	98.75%	11.50%	<u>56.56%</u>
TOPIQ (IAA)	<b>75.00%</b>	22.50%	87.77%	42.81%	98.12%	13.50%	<u>56.62%</u>
TOPIQ (FLIVE)	72.73%	21.75%	87.77%	<u>45.94%</u>	99.38%	13.00%	<b>56.76%</b>
Base Model	73.74%	21.75%	88.30%	43.75%	<b>99.69%</b>	10.50%	56.29%

Table 4. GenEval, more results. The best results are **bold**, the second-best are the third-best are underlined. Table is sorted over "Overall" column.

Additionally, Figure 10 illustrates the relationship between the average scores of four metrics and the input-quality conditions across different IQA-Adapters. All metrics show a monotonic increase in their mean scores, reinforcing the strong correlations shown in Figure 16. This trend is consistent across all IQA-Adapter types, regardless of whether they are trained on IQA models, IAA models, or VLM-based approaches. Starting from a specific target percentile — typically around the 50th percentile — the mean metric scores surpass those of the base model.

## 13. IQA-Adapter as a degradation model

### 13.1. Examples of progressive quality degradation

Figure 17 illustrates the generation results for different percentiles of metric scores on the training dataset. As the percentile decreases, the generated images begin to exhibit various distortions, such as compression artifacts, noise, blurring, and others. These distortions are likely present in the corresponding training datasets for the metrics, causing the trained metrics to become sensitive to them and assign lower scores. Figure 19 presents additional examples of generated distortions under low-quality conditioning.

This property of IQA-Adapter enables leveraging diffu-

sion models as degradation models to generate various distortions, including natural ones. To achieve this, the IQA-Adapter should be trained on a dataset containing the relevant distortions, using as guidance either subjective assessments or a specialized metric sensitive to these distortions. Exploring this approach will be the focus of our future research.

### 13.2. Evaluating distances between high- and low-quality-conditioned generation

To investigate the differences between images generated with varying target quality levels, we estimated the distances between them using four FR IQA metrics: SSIM [80], LPIPS [92], DISTS [18], and PieAPP [60]. SSIM is a classical nonparametric method based on scene statistics, designed to assess structural similarity. LPIPS, on the other hand, is a neural network-based metric that measures similarity as the cosine distance between the features extracted from a pre-trained convolutional network. DISTS refines LPIPS by incorporating additional insensitivity to small image shifts, making it more robust. Lastly, PieAPP demonstrates strong correlations with subjective scores, particularly for the super-resolution (SR) task [8].

We generated 8,200 images with user-generated prompts

Models in IQA-Adapter	FID↓ Full	FID↓ (Top-25%)	FID↓ (Top-10%)	IS↑	CLIP-T↑	CLIP-I↑
LAION-AES	25.84	29.13	34.24	34.59±1.14	26.11	69.12
TRES (FLIVE)	24.11	23.38	27.34	36.74±1.44	25.83	68.68
NIMA (AVA)	24.05	26.03	30.60	38.19±1.02	26.04	69.05
TOPIQ (IAA)	23.93	25.76	30.31	37.95±0.89	26.12	69.08
TOPIQ, LAION-AES	23.51	28.97	28.97	37.30±0.88	26.10	<u>69.13</u>
3xARNIQA, LIQE-MIX (MultiDataset)	23.20	22.73	26.94	37.55±1.37	26.08	68.91
CLIPQA+, LIQE-MIX	23.13	22.97	27.25	<u>38.72±1.73</u>	26.05	68.79
LIQE	23.08	23.50	28.07	37.84±1.12	26.10	68.84
MUSIQ (FLIVE)	23.07	22.68	26.95	37.46±1.05	25.92	68.75
TOPIQ (FLIVE)	22.86	22.66	27.06	37.66±1.04	25.98	68.57
DBCNN	22.75	23.25	27.72	38.04±1.74	26.14	68.73
ARNIQA (KONIQ)	22.72	23.03	27.49	36.58±1.28	26.17	68.74
ARNIQA (KADID)	22.69	23.61	28.36	37.81±1.75	26.02	68.56
MUSIQ (AVA)	22.67	25.12	29.99	37.82±1.26	<u>26.23</u>	<b>69.26</b>
MANIQA (KONIQ)	22.66	23.67	28.08	37.74±0.67	<b>26.32</b>	68.79
HYPER-IQA	22.51	23.14	27.68	37.68±1.18	26.23	68.52
LIQE-MIX	22.46	23.27	27.96	38.07±1.27	26.07	68.86
MUSIQ (KONIQ)	22.45	22.78	27.14	38.24±1.53	26.15	68.65
CLIP-IQA+	22.37	<u>22.27</u>	<b>26.56</b>	37.69±1.60	26.16	69.12
ARNIQA (FLIVE)	22.26	22.30	<u>26.68</u>	<u>38.25±1.47</u>	26.17	<u>69.20</u>
TOPIQ (KONIQ)	<u>21.67</u>	<u>22.21</u>	<u>26.80</u>	37.09±0.63	<u>26.26</u>	68.70
TOPIQ (SPAQ)	<u>21.66</u>	23.03	27.71	37.84±0.87	26.18	68.51
MANIQA (PIPAL)	<b>20.94</b>	<b>22.15</b>	27.15	38.19±0.90	26.08	68.72
Base Model	21.84	23.89	28.88	<b>38.85±1.16</b>	26.01	68.58

Table 5. FID, IS and CLIP scores of the IQA-Adapters trained with different IQA/IAA models on 10k subset of the MS COCO captions. FID-Full is calculated with the full MS COCO training dataset, and FID Top-n% measures FID to the highest-quality subset of MS COCO (as measured by the average score across all IQA/IAA metrics) of the corresponding size. The best results are **bold**, the second-best are the third-best are underlined. Table is sorted over "FID Full" column.

from the Lexica.art website for each target quality level (percentile of metric scores on the training dataset). Figure 11 shows the average distances between corresponding images across different percentiles, measured using the selected FR metrics. As the gap between percentiles increases, the distance between them grows consistently as well. High-quality percentiles (90, 95, 99) are the closest to each other, whereas distant percentiles (e.g., 1 and 99) differ significantly, mostly because of the introduced semantic variations. In contrast, the nearest 2–3 percentiles are quite similar, with differences primarily in small details. Notably, DISTs shows lower differences than LPIPS, suggesting the presence of minor content shifts between images in different percentiles.

## 14. Limitations

IQA-Adapter serves as a guiding mechanism for transferring knowledge from the IQA/IAA domain to generative models. However, the extent of this knowledge transfer is inherently constrained by the capabilities and limitations of current IQA/IAA models. Most existing IQA datasets,

and the models trained on them, are designed to assess the quality of real images, focusing on aesthetical attributes and distortions common for human-generated images. These models often lack the ability to detect distortions specific to generated content, such as unnatural or anatomically incorrect features (e.g., distorted limbs or physically implausible scenes). As a result, these issues may not be adequately penalized in the quality estimates used for guidance, limiting the adapter’s ability to address such generation defects.

Another limitation arises from biases in the training data. The IQA-Adapter can inadvertently learn and reproduce unintended relationships between image content and quality levels present in the dataset. For example, when conditioned on low aesthetic scores, the adapter may generate images with watermarks (see Figure 6, leftmost column), likely because it encountered numerous stock photos with watermarks during training and associated them with lower-quality conditions. Such artifacts highlight the challenge of disentangling genuine quality attributes from dataset-specific correlations.

The training process itself introduces additional chal-

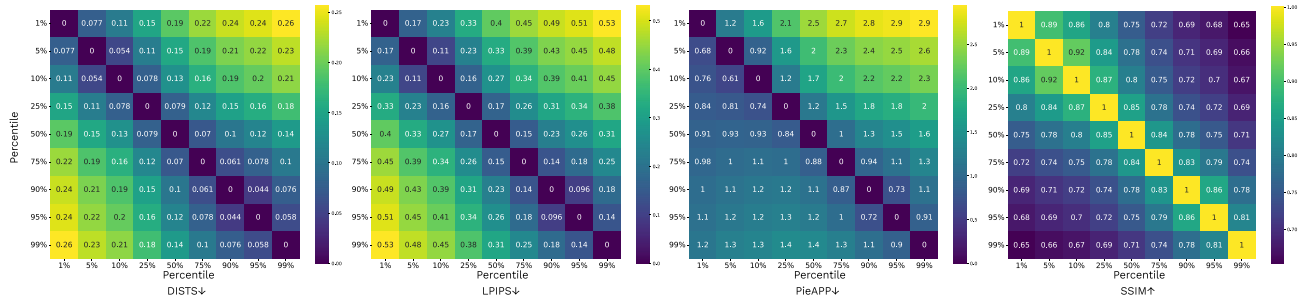


Figure 11. FR IQA metrics distances between images generated with the IQA-Adapter conditioned on different target-quality levels. The IQA-Adapter is trained for HYPER-IQA model.

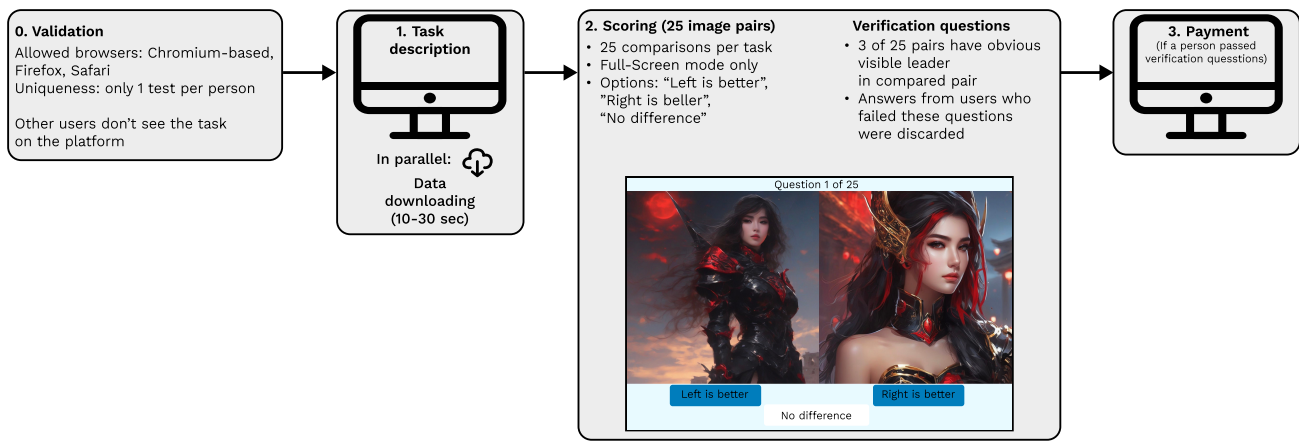


Figure 12. Overall scheme of the subjective study described in Sections 4.3.1 and 15.

lenges. IQA-Adapter training occurs entirely in the latent space of the diffusion model, while the quality scores used for supervision are computed in pixel space. This discrepancy between the latent representations of images (compressed by the model’s VAE encoder) and the pixel-level quality scores can introduce noise into the training process, as the adapter must work with imperfect representations of the input images. Furthermore, the VAE decoder used in the final generation step imposes inherent limitations, as it may introduce artifacts (e.g., blurred text or texture inconsistencies) that the adapter cannot correct.

Finally, while the IQA-Adapter effectively enhances perceptual quality, it may occasionally overemphasize certain features, leading to oversaturated or overly stylized outputs. This is particularly noticeable at high adapter scales, where the balance between preserving generative diversity and increasing quality becomes harder to maintain. Addressing this trade-off remains an open challenge for future work.

### 15. Subjective Study

Our subjective study employed 300 randomly sampled user-generated prompts from the Lexica.art dataset. We used Subjectify.us platform for the evaluation. Overall scheme of

the subjective study and the example of the user interface is demonstrated on Figure 12. During this study, we collected more than 22,300 valid responses of 1,017 unique users: each image-pair was independently assessed by at least 10 unique participants. As we compared 4 models (3 quality-conditions for the IQA-Adapter and the base model), total number of compared image-pairs was  $\frac{4-3}{2} \times 300 = 1800$ . Participants were asked to evaluate the visual quality of the images generated from the same prompts and seeds across all models. Each participant was shown 25 pairs of images from which he had to choose which of them had greater visual quality. The respondent also had the option of “equal quality” in case he could not make a clear choice. Each participant could complete the comparison only once. Of the 25 pairs shown, 3 questions were verification questions and had a clear leader in visual quality. The answers of participants who failed at least one verification question were excluded from the calculation of the results. Comparisons were allowed only in full-screen mode and only through one of the allowed browsers. Before completing the comparison, each participant was shown the following instructions:

Thank you for participating in this evaluation.



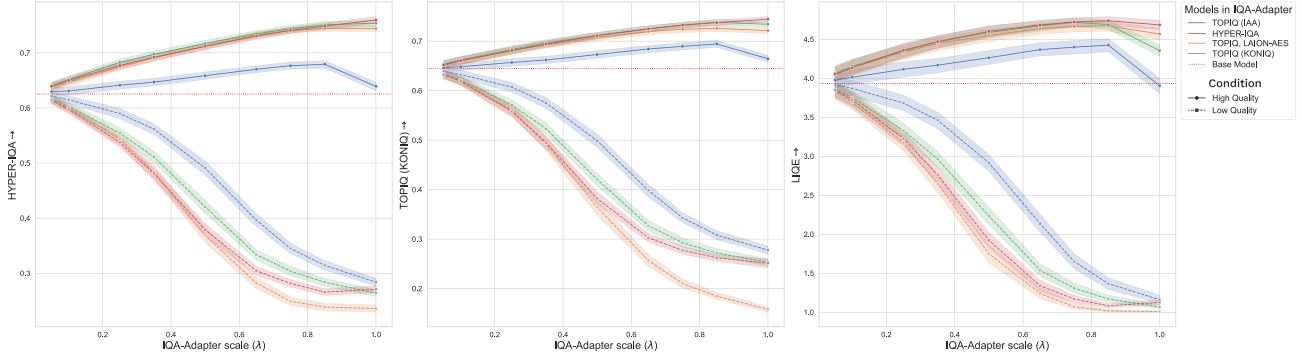


Figure 13. The relationship between image-quality scores (evaluated by the HYPER-IQA, TOPIQ and LIQE metrics) and the adapter scale parameter ( $\lambda$ ) for the IQA-Adapters trained with different target IQA/IAA models and conditioned on low (dashed line) and high (solid line) target quality. For reference, the red dotted line indicates the quality level of the base model. The experiment utilized 300 random user-generated prompts from the Lexica.art dataset.

In this study, you will be shown pairs of images generated by different neural networks from the same text prompt. From each pair, please select the image you believe has higher visual quality. The images may often look quite similar, so in addition to overall "aesthetic appeal," consider factors such as clarity, contrast, brightness, color saturation, and so on. Pay attention to generation defects, such as extra fingers or distorted bodies. If you cannot perceive any difference between the images, you may select "No difference."

The text prompt used to generate the images will not be shown, as this study focuses on evaluating visual quality, and not textual alignment. Please note that the test includes verification questions! In these cases, the differences between the images will be clear, and selecting "indistinguishable quality" will not be considered a valid response."

## 16. Generation with different scales of IQA-Adapter

To evaluate the impact of the adapter scale parameter  $\lambda$  on the visual quality of generated images, we tested IQA-Adapters trained with various IQA/IAA models under both high- and low-quality input conditions. We evaluated 9  $\lambda$  values ranging from 0.05 to 1.0. For each configuration, images were generated using 300 randomly sampled prompts from the Lexica.art dataset. The results are shown in Figure 13.

As  $\lambda$  increases, image quality scores deviate progressively from the base model's levels, aligning with the specified quality condition. Under high-quality conditions, the increase in quality is smooth and resembles a logarithmic

curve for most adapters, reflecting diminishing returns as the base model already achieves relatively high-quality outputs. Beyond a certain threshold for  $\lambda$ , typically around 0.75, further increases cease to improve quality, with excessively high values ( $\lambda > 0.9$ ) introducing artifacts that reduce both visual quality and IQA/IAA scores.

In low-quality conditions, the quality degradation progresses more rapidly, as the adapter has greater freedom to modify the image. The decrease in scores follows a sigmoidal trend: minimal change occurs for small  $\lambda$  values, but the effect accelerates significantly beyond  $\lambda \sim 0.4$  and plateaus at the adapter's limits near  $\lambda \sim 0.75 - 0.85$ . This behavior highlights the non-linear relationship between adapter strength and its impact on image quality, with optimal performance generally observed for  $\lambda$  values in the range of [0.5, 0.75] for both low- and high- quality conditioning.

## 17. Consistency across different seeds

To evaluate the consistency of quality improvements across different seeds, we used 25 random user-generated prompts and sampled 100 random seeds for each, resulting in 2,500 generations per model. The same set of seeds was applied to both the base model and the IQA-Adapter. Figure 14 shows the distributions of relative gains (see Section 4.2) across all generations for adapters trained with different IQA/IAA metrics. Positive values indicate quality improvement relative to the base model for the same seed and prompt.

The results reveal that relative gains follow a unimodal distribution with a positive mean, indicating consistent quality improvement across generations. For some occasional seeds, the base model already achieves near-optimal quality scores and leaving limited room for improvement; in these instances, the adapter introduces negligible changes, resulting in gains close to zero.

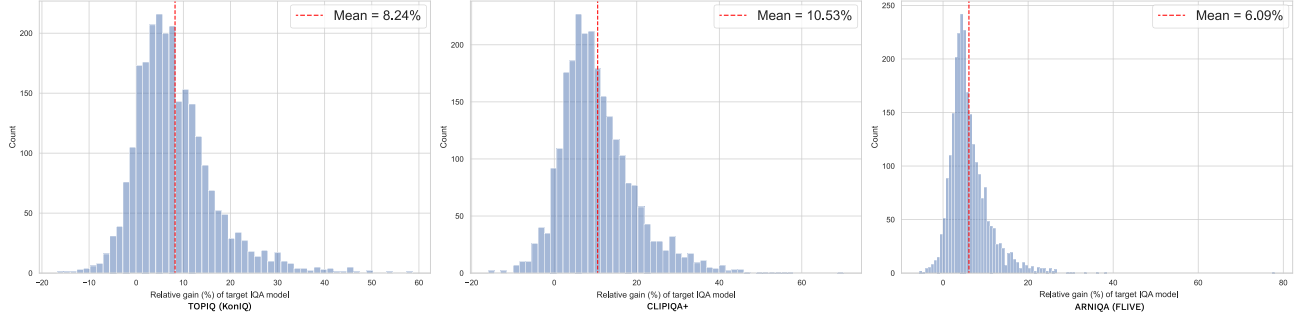


Figure 14. Distributions of relative gains defined in 4.2 across multiple generations with different seeds for IQA-Adapters trained with different IQA models. We use 25 random user-generated prompts and 100 seeds per prompt for this experiment.

Figure 18 illustrates images generated with the same prompt and different seeds, comparing the base model to the IQA-Adapter conditioned on high quality. For this demonstration, we used a strong adapter scale ( $\lambda = 0.75$ ), which introduces noticeable stylization and detailing effects, particularly on high-frequency regions such as hair and textures.

## 18. Generation with different input quality-conditions

Figure 17 illustrates the effects of modulating the IQA-Adapter with progressively higher input quality conditions. From left to right, the target quality corresponds to increasing percentiles (1st to 99th) of the target model’s scores on the training dataset. As the target quality increases, the generated images exhibit enhanced detail and clarity, demonstrating the adapter’s ability to shift image quality in alignment with the specified condition.

## 19. More Examples of adversarial patterns

Figure 20 presents a comparison of images generated by the base model (left column), the gradient-based method (middle column), and the IQA-Adapter (right column), alongside GradCAM visualizations of the target IQA model used for both gradient-based guidance and IQA-Adapter training. The gradient-based method often introduces artifacts that significantly alter the attention maps of the target model, inflating the quality score by exploiting architectural vulnerabilities. For instance, with the TOPIQ model (first row), new “adversarial” objects are added to the image, capturing the model’s attention and artificially boosting its scores. For TRES, grid-like patterns are generated that divert the model’s focus away from the adversarial region. Similarly, with NIMA and HYPER-IQA, the method saturates the image with high-frequency details and color variations, dispersing the model’s focus.

In contrast, the IQA-Adapter effectively preserves the target model’s saliency maps, maintaining focus on relevant

objects in the scene, even when the image undergoes structural modifications.

## 20. Positional Encoding

Given that the quality metrics used as input for the IQA-Adapter form a low-dimensional representation (e.g., a 2D space for quality and aesthetics, as shown in Figures 1 and 6), we explored the use of positional encoding to enrich these inputs. Inspired by the sinusoidal encoding strategy employed in NeRFs[51] and timestamp encoding in Stable Diffusion models[62], we applied the following transformation to each input IQA/IAA value independently:

$$\gamma(x) = (x, \sin(2^0\pi x), \cos(2^0\pi x), \dots, \sin(2^{L-1}\pi x), \cos(2^{L-1}\pi x)),$$

where  $x$  is the input value, and  $L$  controls the number of additional components in the representation. All IQA/IAA inputs were normalized to zero mean and unit variance prior to this transformation.

We hypothesized that positional encoding would enhance the model’s sensitivity to subtle quality variations, allowing for more fine-grained control over output quality without affecting behavior at the edges of the input range. However, our experiments demonstrated that positional encoding had minimal impact on the model’s behavior.

To evaluate this, we conducted experiments where the IQA-Adapter was modulated on the input quality condition, as described in Sections 4.3 and 17. Using a dataset of user-generated prompts from Lexica.art, we compared IQA-Adapters with and without positional encoding across a range of evaluation metrics. The results, shown in Figure 15, indicate that positional encoding produced outcomes nearly identical to those of the baseline IQA-Adapter, regardless of the value of  $L$ .

Although our experiments did not reveal significant benefits from positional encoding for the quality-conditioning task, we believe there may be potential for improvement

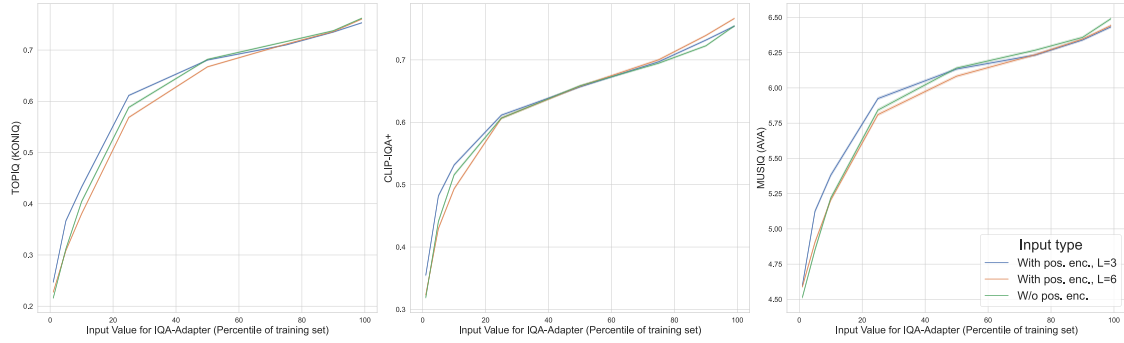


Figure 15. Results of the IQA-Adapter modulation on input quality-condition for different types of input preprocessing with positional encoding. For all evaluated types, adapter was trained with TOPIQ (KONIQ) model.

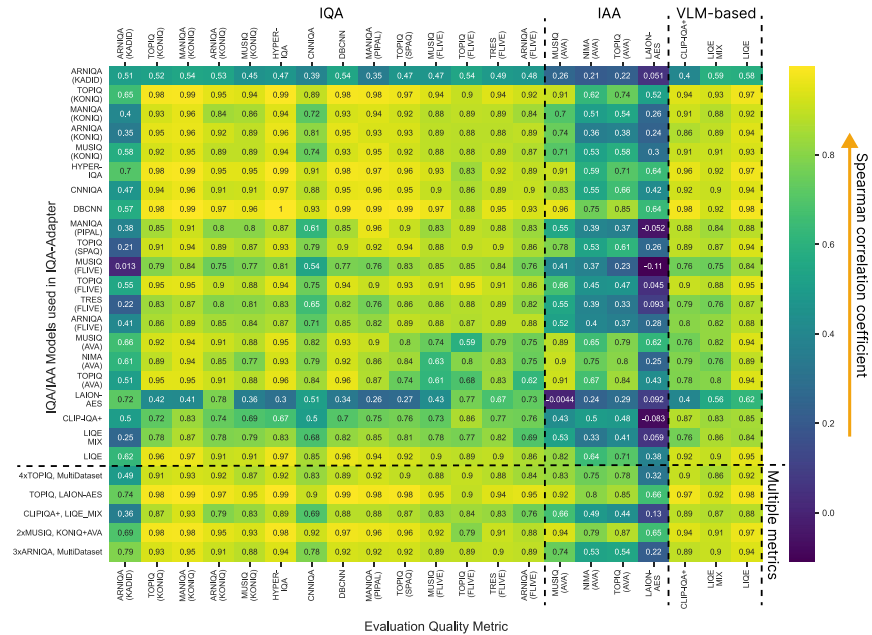


Figure 16. Correlations between input quality-conditions (represented as a percentile of target IQA/IAA model on the training dataset) and metric scores for the IQA-Adapters trained with different IQA/IAA models.

with alternative encoding strategies. For instance, rotary positional embeddings (RoPE)[73], which have shown success in recent large language models, could be a promising direction. We leave the exploration of such strategies for future research.





Figure 17. Visualization of generations with different target-quality conditions with IQA-Adapters trained with different IQA/IAA models. Input quality increases from left (1-st percentile of the training set) to right (99-th percentile).



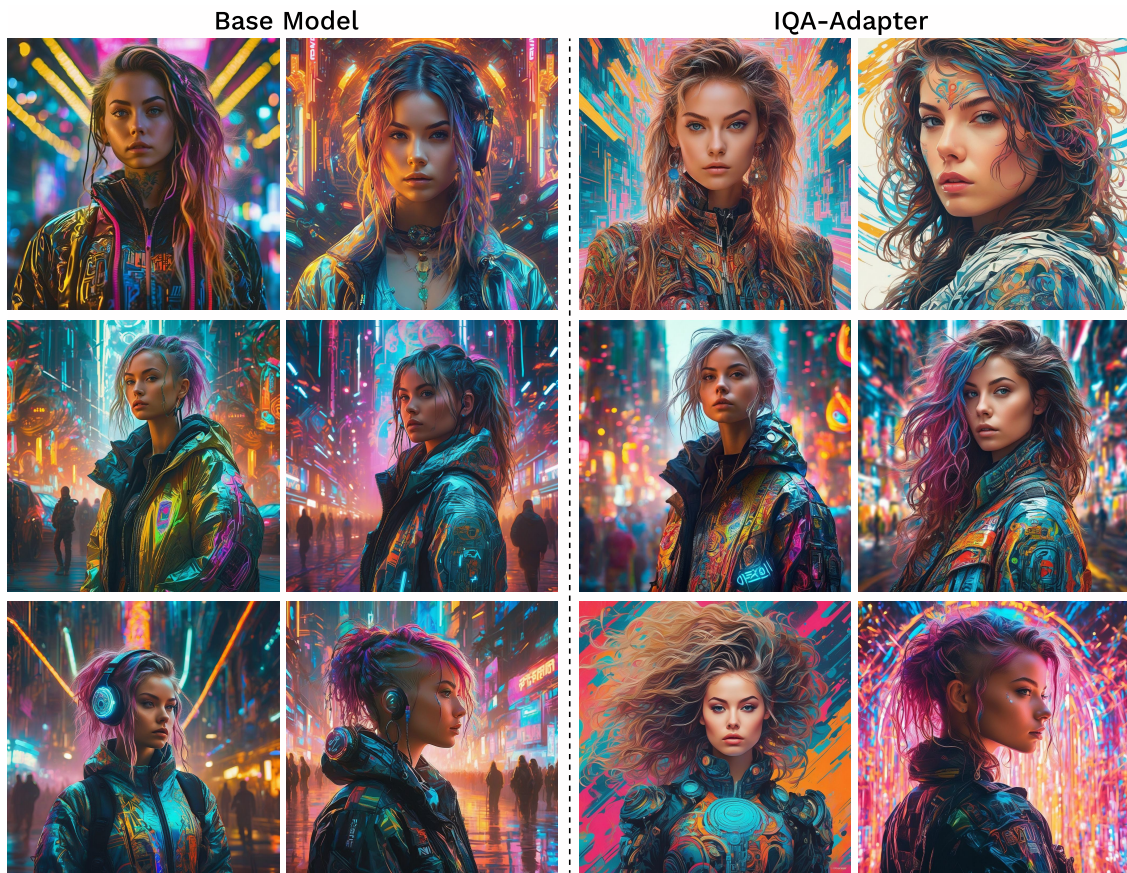


Figure 18. Examples of images generated with and without IQA-Adapter with the same prompt. In this experiment, we employed the IQA-Adapter trained using the CLIP-IQA+ and LIQE-MIX models.

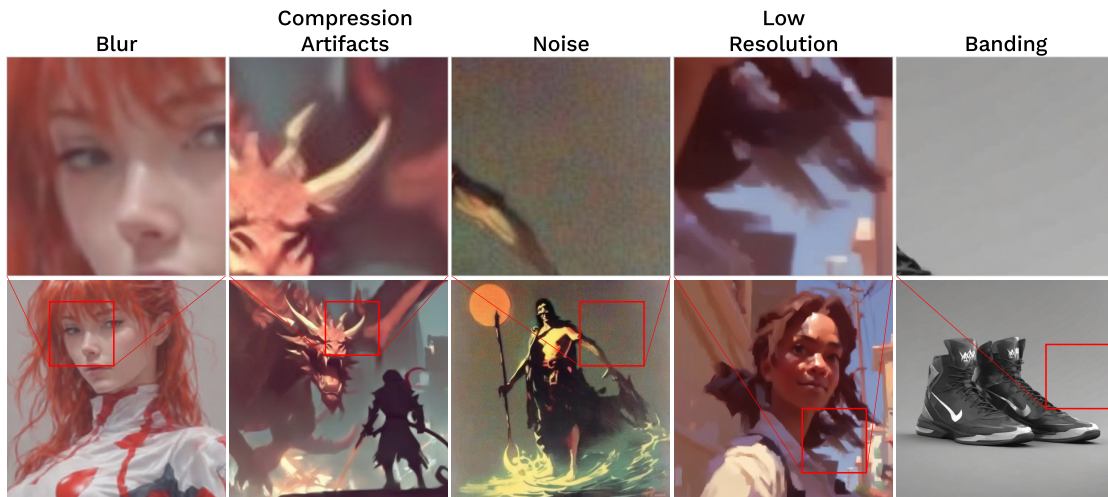


Figure 19. Examples of images generated with IQA-Adapter conditioned on **low** quality. IQA-Adapter is able to reproduce various distortions present in the training dataset.



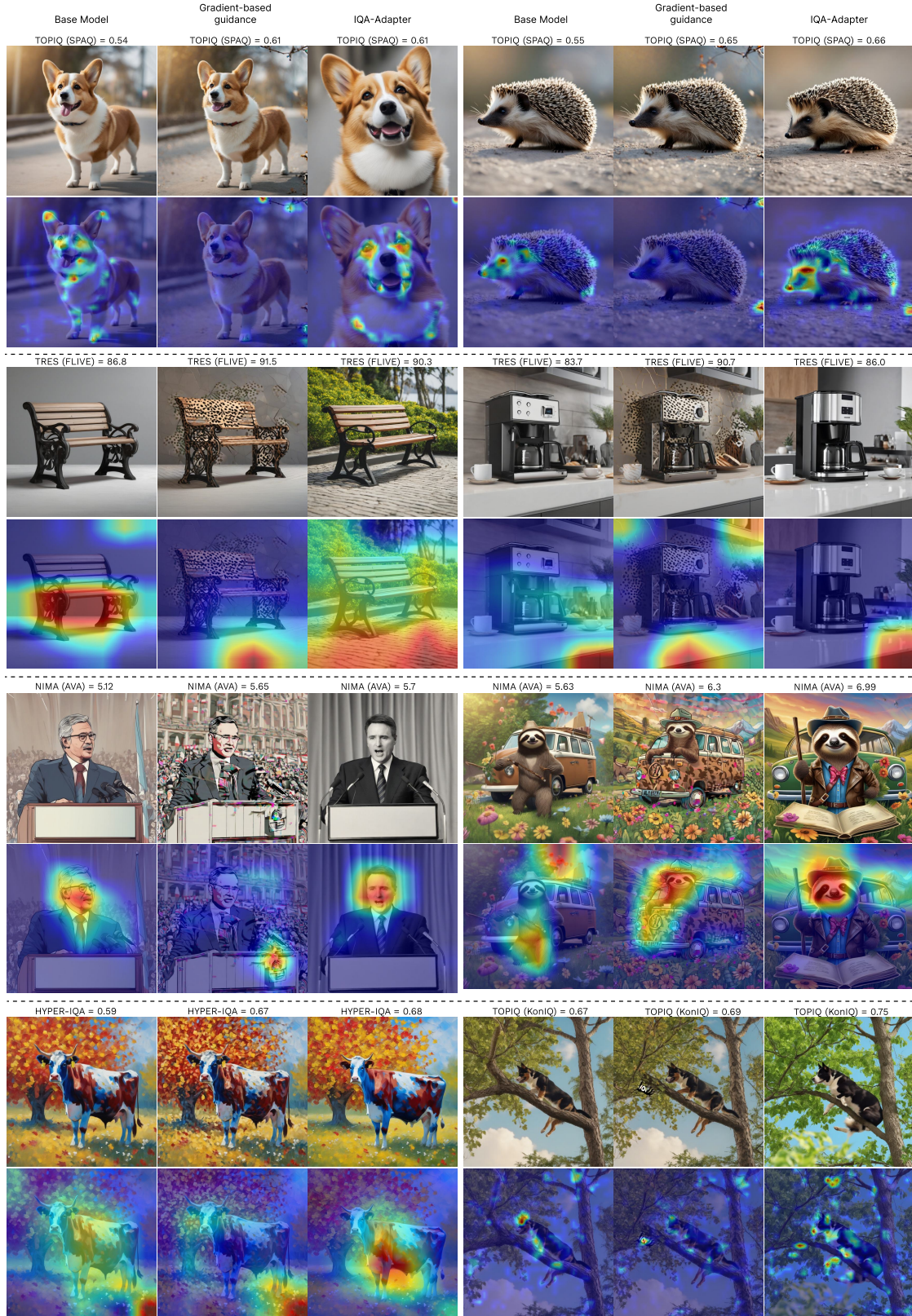


Figure 20. The comparison of adversarial examples generated with the gradient-based method (middle column) alongside outputs from the base model (left column) and the IQA-Adapter (right column), accompanied by their corresponding quality scores. Different rows represent different target IQA/IAA models in the gradient-based method and IQA-Adapter. Even-numbered rows display GradCAM visualizations of the target IQA model applied to the images in the respective columns. The prompts are taken from the PartiPrompts dataset.